Atmos. Meas. Tech. Discuss., https://doi.org/10.5194/amt-2018-47
Manuscript under review for journal Atmos. Meas. Tech.
Discussion started: 23 February 2018

Atmospheric Measurement Techniques Discussions

HOVERCAT: A novel aerial system for evaluation of aerosol-cloud interactions

Jessie M. Creamean[1,2], Katherine M. Primm[1], Margaret A. Tolbert[1], Emrys G. Hall[1,3], Jim Wendell[3], Allen Jordan[1,3], Patrick J. Sheridan[3], Jedediah Smith[4], Russell C. Schnell[3]

[1]Cooperative Institute for Research in Environmental Sciences, University of Colorado, Boulder, CO, 80309, USA
[2]Physical Sciences Division, National Oceanic and Atmospheric Administration, Boulder, CO, 80305, USA
[3]Global Monitoring Division, National Oceanic and Atmospheric Administration, Boulder, CO, 80305, USA
[4]Smith & Williamson, Corvallis, OR, 97330, USA

Correspondence to: Jessie M. Creamean (jessie.creamean@noaa.gov)

Abstract. Aerosols have a profound impact on cloud microphysics through their ability to serve as ice nucleating particles (INPs). As a result, cloud radiative properties and precipitation processes are modulated by such aerosol-cloud interactions. However, one of the largest uncertainties associated with atmospheric processes is the indirect effect of aerosols on clouds. The need for more advanced observations of INPs in the atmospheric vertical profile is apparent, yet most ice nucleation measurements are conducted at the ground or during infrequent and intensive airborne field campaigns. Here, we describe a novel measurement platform that is less expensive and smaller (< 5 kg) when compared to traditional aircraft platforms. HOVERCAT (Honing On VERtical Cloud and Aerosol properTies) flew a successful aerosol collection flight in Colorado, USA up to 2.6 km above mean sea level (1.1 km above ground level). HOVERCAT consists of the Boomerang Balloon Flight Control System that has the capability to "hover" at desired altitudes and an aerosol module that includes an optical particle counter for size distributions (0.38 – 17 µm in diameter) and a time-resolved sampler that collects up to ten filter samples for offline ice nucleation and aerosol analyses. During the May 2017 test flight, total particle concentrations were highest closest to the ground (up to 50 cm^{-3} at < 50 m above ground level) and up to 2 in 10^2 particles were ice nucleation active in the immersion mode (at −23 °C). The warmest temperature immersion and deposition mode INPs (observed up to −6 °C and −40.4 °C, respectively) were observed closest to the ground, but overall INP concentrations did not exhibit an inverse correlation with increasing altitude. HOVERCAT is a prototype that can be further modified for other airborne platforms, including tethered balloon and unmanned aerial systems. The versatility of HOVERCAT affords future opportunities to profile the atmospheric column for more routine evaluations of aerosol-cloud interactions.

1 Introduction

Some of the least understood atmospheric processes are aerosol-cloud interactions, and specifically, those with aerosols that serve as ice nucleating particles (INPs) (Boucher et al., 2013). Formation and microphysical modulation of cloud droplets and ice crystals is highly dependent upon the types and number of aerosols that serve as cloud condensation nuclei (CCN)

and INPs. In the absence of CCN and INPs, clouds would in theory require > 400% humidity and < −36 °C to form droplets and ice crystals, respectively; conditions atypical of mixed-phase clouds (Pruppacher and Klett, 1997). Aerosol-induced microphysical modifications influence cloud lifetime and albedo (Morrison et al., 2005), as well as the production of more or less precipitation, particularly in mixed-phase cloud systems. INPs nucleate ice through pathways dependent upon temperature, saturation with respect to ice, and the INP type (Hoose and Möhler, 2012). The modes of heterogeneous ice nucleation include: 1) condensation freezing whereby ice is formed concurrently with the initial formation of liquid on CCN at supercooled temperatures, 2) immersion freezing whereby an INP is immersed in an aqueous solution or water droplet via activation of CCN during liquid cloud formation, 3) contact freezing whereby an INP approaches the air–water interface of a droplet (e.g., via a collision) and initiates freezing, and 4) deposition freezing whereby ice is nucleated from supersaturated vapour with respect to ice (RH_i > 100%) on an INP directly (Hoose and Möhler, 2012; Coluzza et al., 2017; Cziczo et al., 2017; Kanji et al., 2017).

Immersion freezing is the most relevant to mixed-phase cloud ice formation and requires that INPs initially serve as, or in conjunction with, CCN, whereas deposition freezing is prevalent in mixed-phase and dominant in cirrus cloud ice formation (Kanji et al., 2017). Aerosols such as mineral dust, soil dust, sea salt, volcanic ash, black carbon from wildfires, and primary biological aerosol particles (PBAPs) have been shown to serve as INPs (DeMott et al., 1999; Petters et al., 2009; Conen et al., 2011; Hoose and Möhler, 2012; Murray et al., 2012; McCluskey et al., 2014; Cziczo et al., 2017). Among these, dust and PBAPs are the most adroit INPs found in the atmosphere (Murray et al., 2012; Cziczo et al., 2017). Dust is the most atmospherically-abundant INP, forming ice as warm as −10 °C, but primarily at temperatures < −15 °C (Hoose and Möhler, 2012; Murray et al., 2012). On the other hand, PBAPs are relatively rare in the atmosphere, but can form ice as warm as −1 °C (Vali and Schnell, 1975; Schnell and Vali, 1976; Vali et al., 1976; Despres et al., 2012). However, constraining aerosol-cloud impacts in models ranging from the cloud-resolving to climate scales, specifically when parameterizing INPs, remains a significant challenge due to limited observations (DeMott et al., 2010; Coluzza et al., 2017; Cziczo et al., 2017).

A number of previous ground-based field measurements dating back to the 1950s have provided noteworthy advancements in understanding the sources and efficiencies of INPs (e.g., Mossop, 1963; Jayaweera and Flanagan, 1982; Durant et al., 2008; Petters et al., 2009; Prenni et al., 2009b; Bigg, 2011; Garcia et al., 2012; Murray et al., 2012; Huffman et al., 2013; Prenni et al., 2013; McCluskey et al., 2014; Mason et al., 2015). Further, previous work has evaluated INP concentrations and at times composition in detritus, soil, water from lakes and oceans, surface microlayers, and precipitation samples to assess INP sources (e.g., Schnell and Vali, 1972, 1973, 1975; Schnell, 1977; Creamean et al., 2014; O'Sullivan et al., 2014; Tobo et al., 2014; Petters and Wright, 2015; Stopelli et al., 2015; Conen et al., 2016; DeMott et al., 2016; Hill et al., 2016; Moffett, 2016; Irish et al., 2017; Pietsch et al., 2017; Pouzet et al., 2017). Analysis of INPs in precipitation samples take a step in the direction of vertical profiling of INPs, making the assumption that the INPs in precipitation are what initiated ice formation in the clouds above; however, there are caveats associated with artefacts from scavenging during raindrop or

snowflake descent, aerosolization methods, and redistribution of residue particles in collected liquid precipitation samples (Creamean et al., 2014; Petters and Wright, 2015; Hanlon et al., 2017).

Although observations at the ground afford detailed information regarding the characterization of INP sources, they may not be representative of INPs in the atmospheric column, where they have the direct ability to impact cloud ice formation processes and may originate from a range of local to long-range transported sources. As a result, several INP quantification and characterization studies have been conducted in clouds at mountaintop atmospheric research facilities, such as Storm Peak Laboratory in the United States (Cziczo et al., 2004; Richardson et al., 2007; Baustian et al., 2012), Puy de Dôme in France (Joly et al., 2013; Joly et al., 2014), and Jungfraujoch in Switzerland (Chou et al., 2011; Conen et al., 2015; Stopelli et al., 2016; Stopelli et al., 2017). Such studies provide routine or long-term measurements of INPs in clouds, yet one disadvantage is that profiling is not possible. Vertical profiling of INPs can serve as a connection between the ground and various altitudes below, in, and above cloud. Targeted aircraft campaigns have helped explain the role of INPs in cloud ice formation at all levels from below cloud, cloud base, in-cloud, and cloud top (e.g., Schnell, 1982; Rogers et al., 1998; Curry et al., 2000; Rogers et al., 2001; DeMott et al., 2003; Pratt et al., 2009; Prenni et al., 2009a; DeMott et al., 2010; Avramov et al., 2011; Creamean et al., 2013). Although such campaigns yield results crucial for understanding the vertical distribution of INPs in cloudy environments, they are intensive with regard to personnel, cost, and time.

Overall, a key gap in ice nucleation research is routine vertical profiling of INP abundance, efficiency, and chemical and physical characterization (Coluzza et al., 2017). Tropospheric measurements via balloon-based systems have been a desirable means of measuring aerosol properties on an inexpensive and thus, more frequent basis. However, such measurements can be limited in terms of time, measurements made, or location. For example, long-term records of tropospheric aerosol particle size distributions have been reported in Wyoming, United States (i.e., 20 years) (Hofmann, 1993). The same launched balloon system was deployed in Antarctica, demonstrating the utility of this platform in multiple environments (Hofmann et al., 1989). Particle size distributions have also been measured via launched balloons in several locations in China using optical particle counters (Iwasaka et al., 2003; Kim et al., 2003; Tobo et al., 2007). One major caveat with these studies is that it is not clear if the balloon systems were retrievable, given their maximum flight ceilings were located well into the stratosphere. In addition, the launched balloon platforms provide information on 1 – 2 aerosol profiles (i.e., ascent and sometimes descent) and are limited by payload weight. Particle spectrometers have also been deployed and retrieved on tethered balloon systems (Maletto et al., 2003; Siebert et al., 2004; Wehner et al., 2007; Greenberg et al., 2009; Renard et al., 2016; de Boer et al., 2018), affording information on aerosol layer locations and evolution by means of multiple profiles. A few studies have deployed miniature aerosol filter samplers on launched or tethered balloon systems, yielding information on aerosol chemistry (Rankin and Wolff, 2002; Hara et al., 2011); however, such samplers contain one filter per flight, thus providing information on aerosol properties at only one altitude (i.e., not a profile). In general, tethered balloons can handle much larger payloads than launched systems, but are limited to lower altitudes (i.e., up

to approximately 2 km above ground level (AGL)) and have wind condition limitations, thus may not be ideal for sampling at various levels where clouds exist.

Overall, both launched and tethered balloon platforms have their advantages and disadvantages in terms of flight ceiling, profiling, retrieveability, and payload restrictions. Additionally, to our knowledge, there have been no measurements of INPs via any balloon platform. A solution to reduce the limitations of these methods is a launched balloon system that can be controlled in terms of altitude, to afford multiple profiling and payload retrieval capabilities, and a system that collects aerosol loadings sufficient for altitude-resolved offline ice nucleation measurements. Here, we present an experimental launched balloon system, called HOVERCAT (Honing On VERtical Cloud and Aerosol properTies), that possesses such capabilities.

2 Methods

The first prototype of HOVERCAT was recently built and tested in Colorado, United States, consisting of a novel balloon platform capable of 'hovering' at desired altitudes called the Boomerang Balloon Flight Control System (BBFCS). Additionally, HOVERCAT contains an aerosol module for measuring real-time particle size distributions and a time-resolved filter sampler for aerosol collection for offline ice nucleation analyses. The current version of HOVERCAT is experimental, thus we consider it as in Phase I of its development, and is described herein. As discussed later, we provide future directions for modification and improvement of HOVERCAT for future deployments.

2.1 Balloon platform

BBFCS is a real-time, remote device that allows the user to control the altitude of standard latex weather balloons (Figure 1a). The primary features are a lift-gas vent valve in the control module that permits negative buoyancy adjustments and a sand ballaster (i.e., ballast module) that permits positive buoyancy adjustments. Buoyancy adjustments as small as 5 g of lift are possible. Two-way communication is achieved through a 70-cm line-of-sight LoRa radio link. The system features a 1/4W transceiver that uses a low baud rate and a slow 4-second time-division multiple access (TDMA) cycle to achieve ranges in excess of 300 km. The system also features redundant termination methods, anti-collision strobes, positioning, and flight sensors. A recovery parachute is included for emergency termination and faster fall speeds than slow balloon deflation. The BBFCS was manually controlled for this project. We utilized a software interface on a ground-based computer to analyse the real-time flight conditions and send the necessary buoyancy control commands to achieve the desired flight profile. Early morning launches were conducted to maximize the calm low-troposphere atmospheric conditions as flight control is much easier in such conditions. Because this project entailed low-altitude flights that did not exceed 9.6 km above mean sea level (AMSL), 300 g latex balloons were used. These relatively small balloons, for a 3.9-kg payload, ensured that the envelope was always under tension and would expel lift-gas whenever the vent valve was opened, while ensuring that the

burst altitude was above the expected operational altitude. Burst altitude was calculated to be 13 – 14 km AMSL depending on how much lift gas had been vented. The BBFCS is designed to allow Federal Aviation Administration (FAA) part 101 exempt flights, even when carrying a reasonably-sized payload (i.e., total payload weight of less than 5.5 kg and no one module greater than 2.3 kg).

2.2 Aerosol module

The aerosol module package contains: 1) an optical particle counter (Alphasense OPC-N2) for particle size distributions (16 size bins for 0.38 – 17 µm in diameter) and estimated particle mass concentrations with optical diameters ≤ 1, 2.5, and 10 µm (PM_1, $PM_{2.5}$, and PM_{10}, respectively) and 2) the National Oceanic and Atmospheric Administration (NOAA)-built miniaturized Time-Resolved Aerosol Particle Sampler (TRAPS) for collection of up to 10 samples. The OPC-N2 operates at 175 mA in operation mode and weighs 105 g. Flow rates are adjusted based on ambient pressure to maintain a 1.2-L min^{-1} flow using a patented 'pump-less' design. Data are stored on a microprocessor within the OPC during collection. The TRAPS design is based on the filter components of the NOAA Continuous Light Absorption Photometer (CLAP), without the optical components and measurements (Ogren et al., 2017). It is connected to a small 12 VDC vacuum pump (Brailsford & Co., Inc. TD-4X2N), which nominally enables a flow rate of approximately 1.2±0.1 L min^{-1} through the TRAPS when a 47-mm filter is in place. A Honeywell AWM43600V mass flow meter measures sample flow rate. Ten miniature solenoid valves select the active sample spot and are controlled by an on-board microprocessor preselected for the desired time resolution, which was 30 minutes per sample spot for the HOVERCAT test flights. The TRAPS flow rate at 30 minutes provides approximately 40 total litres of air through each spot, which is ideal for measuring more realistic INP concentrations (Mossop and Thorndike, 1966). Sample loaded spots average to a coverage area of 19.9 mm^2 (equates to a spot diameter of approximately 4.46 mm). The TRAPS collects particles in the 1 nm – 10 µm aerodynamic diameter range, with particle losses of less than 10% for 5 nm – 7 µm particles and less than 1% for 30 nm – 2.5 µm particles at 1.0 L min^{-1} (Ogren et al., 2017).

The TRAPS, micropump, and OPC are all operated by battery: the TRAPS and micropump run off a battery pack containing three 18650 rechargeable Li-ion batteries (Panasonic NCR18650B, 12 V output, 3400 mAh) and the OPC runs off one rechargeable battery (Anker PowerCore 5000, 5 V output, 5000 mAh). The OPC can operate for several days on its portable battery, while the TRAPS and pump can operate for up to 5 hours on its battery pack. Both the TRAPS and OPC are connected to inlets composed of an 8-inch segment of ¼-inch ID black conductive tubing connected to a stainless-steel funnel (5 cm in diameter) with the opening covered with stainless steel mesh. All components are seated in a foam enclosure with removable lid and inlets extending out of the bottom (Figure 1b).

2.4 Test flight details

The overall launch mass of HOVERCAT was 4250 g with 450 g of free lift to achieve an initial 3 m s^{-1} ascent rate. System masses were: 350 g for the balloon and connection spindle, 900 g for the BBFCS and parachute, 2300 g for the aerosol module, and 700 g of ballast. Initial flight planning called for a 5-step flight profile with 500-m altitude steps. This allocated 100 g of ballast per step, 1.5 m s^{-1} anticipated ascent rate between steps, with a 200-g reserve for the flight to help maintain the desired altitude. The flight train for this project consisted, from top to bottom: latex balloon, valve and flight computer modules, 500 mm of line, aerosol module, 500 mm of line, and ballast module (Figure 1c). The recovery parachute was attached to the bottom of the flight computer module and hung off to the side. The parachute's apex was attached to the termination clamp and was released by this clamp during termination or by aerodynamic drag if the balloon had prematurely burst. The OPC was started during balloon inflation and the TRAPS and micropump were started via Bluetooth just prior to take off. HOVERCAT also had two miniature cameras (Mobius Basic ActionCam with wide angle lens) mounted to and facing the BBFCS valve module and aerosol module for time lapse photos during take-off, flight, and landing.

Three test flights were conducted in central Colorado during 24 – 26 May 2017. Two of the three flights had instrument operational issues (i.e., 24 and 26 May), so only data from the 25 May flight is presented herein. Briefly, communications were lost during the 24 May flight and as a result, controlling the valve and ballast modules was not possible. HOVERCAT reached 9.6 km AMSL and ambient pressure was too low for the TRAPS pump to operate. The 26 May flight reached > 2 km AMSL, in which the TRAPS pump also did not operate correctly. For both the 24 and 26 May flights, the total volume of air pulled through the filters was 1 – 12 L above 2.5 km AMSL (1.1 km AGL), equating to loadings too low for offline analyses (i.e., calculated INP concentrations were below detection limits). Based on the successful 25 May flight and unsuccessful flights on 24 and 26 May, we have concluded that in its current configuration, HOVERCAT can operate below 2.5 km AMSL, otherwise at the low pressures, the current micropump cannot generate sufficient flow. New, higher volume pumps are being tested.

The 3-dimensional flight path for 25 May is shown in Figure 2. The horizontal distance between launch and landing was 16.8 km, bird's eye view. Conditions were partly cloudy with surface air temperatures ranging from 16 – 21 °C, relative humidity from 35 – 47%, and wind speeds from 2 – 3 m s^{-1} from the north and south (hourly meteorological data during flight times obtained from the Colorado Department of Public Health and Environment (CDPHE) at the Boulder Reservoir site; 40.07°N, 105.22°W; https://www.colorado.gov/pacific/cdphe/data). HOVERCAT did not fly through the clouds present that day, but remained below cloud base, based on visual identification of the system while tracking in real-time (i.e., HOVERCAT was always in line-of-sight).

2.3 Offline ice nucleation analyses

2.3.1 Drop freezing assay for immersion mode ice nucleation

For the 25 May flight, aerosol samples were collected on 47 mm filters (Pallflex® EmFab™). Pre-treatment of the filters by means of a 6 N nitric acid bath (Certified ACS Plus, Fisher Scientific), 3 times rinse with ultrapure water (UPW; Barnstead™ Smart2Pure™ 6 UV/UF), and baking at 150 °C for 30 minutes, was conducted to remove possible filter INP artefacts. Out of the filters tested, EmFab™ possessed the lowest contribution from artefacts compared to cellulose nitrate and polytetrafluoroethylene and survived the pre-treatment process.

Immersion mode freezing was tested using a drop freezing assay (DFA) cold plate apparatus. This cold plate technique was based on previous but slightly modified apparatuses (Wright and Petters, 2013; Stopelli et al., 2014; Hill et al., 2016; Tobo, 2016). For brevity, we call this system the NOAA Drop Freezing Cold Plate (DFCP). Following collection and prior to analysis, sample filters were stored frozen for approximately six months. After removing from the freezer, each sample spot was carefully cut and separated from the 25 May filter; only six spots (i.e., samples) were successfully collected before the battery died. Each spot was placed is a 29-mL sterile Whirlpak® bag with 2 mL of UPW to resuspend particles deposited on the filter. The bags were sealed and shaken at 500 rpm for two hours (Bowers et al., 2009). Copper discs (76 mm in diameter, 3.2 mm thick) were prepared by cleaning with isopropanol (99.5% ACS Grade, LabChem. Inc.), then coated with a thin layer of petrolatum (100%, Vaseline®) (Bowers et al., 2009; Tobo, 2016). Three of the spots on the filter had visible aerosol deposits that were successfully transferred to the UPW (i.e., based on visual identification).

Following sample preparation, a sterile, single-use syringe was used to draw 0.25 mL of the suspension and 100 drops were pipetted onto the petrolatum-coated copper disc, creating an array of ~2.5-µL aliquots. Drops were visually inspected for size; however, it is possible not all drops were the same exact volume, which could lead to a small level of indeterminable uncertainty. However, previous studies have elucidated that drops need to be orders of magnitude different in volume to significantly perturb the freezing temperature from drop size, alone (Bigg, 1953; Langham and Mason, 1958; Hader et al., 2014). The copper disc was then placed on a thermoelectric cold plate (Aldrich®) and covered with a transparent plastic dome. Small holes in the side of the dome and copper disc permitted placement of up to four temperature probes using an Omega™ thermometer/data logger (RDXL4SD). The Omega™ meter has a 0.1 °C resolution and accuracy of ± (0.4% + 0.5 ºC) for the K sensor types used. During the test, the cold plate was cooled at 1 – 10 °C min^{-1} from room temperature until all drops on the plate were frozen. Control experiments with ultrapure water at various cooling rates within this range show no discernible dependency of drop freezing on cooling rate, akin to previous works (Vali and Stansbury, 1966; Wright and Petters, 2013). Frozen drops were detected visually, but recorded through software written in-house, providing the freezing temperature and cooling rate of each drop frozen. The test continued until all 100 drops were frozen, typically occurring around −30 °C. Each sample was tested three times with 100 new drops for each test. From each test, the fraction frozen and percentage of detected frozen drops were calculated. The results from the triplicate tests are then binned every 0.5 °C to produce one spectrum per sample.

Although the methodology behind DFA is well established, control experiments were conducted with UPW for full system characterization of the DFCP. First, temperature differences were measured within the range of cooling rates using UPW on petrolatum-coated copper discs between the centre of the disc (thermocouple inserted in a small diameter hole in the side of the disk) and a drop on top of the plate with a thermocouple inserted into the drop (Figure 3). As expected based on previous work (Vali and Stansbury, 1966; Wright and Petters, 2013), there was no dependence of the temperature difference on cooling rate, but on average, the drop temperature was 0.33±0.15 °C warmer than the centre of the plate. Thus, a +0.33 °C correction factor was added to any temperature herein and an uncertainty of 0.15 °C was added to the probe accuracy uncertainty.

Second, various hydrophobic coatings with UPW were tested for the best combination of materials to use with the least influence from artefacts (Figure 4). Materials tested were chosen based on those used in previous work and included: 1) direct petrolatum (Tobo, 2016), 2) 15% w/v petrolatum in xylenes (Certified ACS Reagent Grade, Ricca Chemical) (Bowers et al., 2009), 3) silicone fluid (710 fluid, Dow Corning®) (Polen et al., 2016), and 4) squalene (≥ 98%, Sigma-Aldrich®) (Wright and Petters, 2013; Wright et al., 2013; Hader et al., 2014). The silicone fluid was difficult to use for cold plate experimentation because droplets would coalesce during the experiment and freezing detection by eye was difficult due to the glare of the substance. Squalene was less viscous than the silicone fluid, inducing more drop coalescence but freezing detection was easier than the silicone fluid. Both materials remained in the fluid state, thus are not ideal for direct cold plate use, but have been proven suitable for cold stages that use covered sample dishes or trays and smaller drop sizes (Wright and Petters, 2013; Wright et al., 2013; Hader et al., 2014; Polen et al., 2016). The petrolatum and xylenes solution creates a thin layer of petrolatum after drying to evaporate the xylenes and alleviate the coalescence problem; however, as evidenced by the freezing spectra in Figure 4, is not the best option in terms of limiting artefacts. To summarize, a hydrophobic coating is needed on the copper plate and the option with the least influence from contaminants is direct petrolatum smeared onto the plate using UPW.

Last, the effect of drop size was tested using UPW and petrolatum-coated copper plates (Figure 5). Normally, 2.5-µL drops are created by hand using a sterile syringe. Because such drops are created without the use of a pipette, possible small variations in drop volume may occur. The same volume drops were created with a pipette and sterile tips and tested against syringe drops. Additionally, tests with 1.5-µL and 5.0-µL drops were conducted to evaluate the effects of larger changes in volume. One major caveat with the pipette technique is that it takes substantially more time to create the arrays of 100 drops (approximately five times slower than the syringe method). Overall, the best method in terms of onset freezing temperatures and fraction frozen was the 2.5-µL drops created via syringe. This test was comparable in terms of fraction frozen to the 1.5-µL drops colder than −21 °C. One possible explanation for the higher onset temperature and higher concentrations of impurities in the 2.5-µL pipetted drops as compared to the 2.5-µL syringed drops is contamination from the pipette tips. The 5.0-µL test demonstrated that drops of this size are too large such that they induce freezing at warmer temperatures and are

subject to large variability—in theory, the larger the drop volume, the larger the abundance of impurities within a single drop that may facilitate ice formation (Bigg, 1953). Overall, our drop size tests demonstrate the efficiency and reliability of 2.5-µL drops created via syringe.

Out of the 100 drops for each test, 95±5% on average (ranging between 84 – 100%) were detected as frozen and recorded from all tests (Figure 6). Some of the tests within the same sample were reproducible within error, demonstrating the reliability of the method (e.g., samples 1 and 3). However, variability from test-to-test within the same sample could occur due to: 1) detection of rarer INPs at specific temperatures during 1 – 2 of the tests or 2) uncertainties arising from instrumental artefacts, such as contamination between tests. These results demonstrate the importance of running triplicate (or more) tests for DFA techniques—to capture some of the rarer INPs that may exist in the samples or account for test-to-test variabilities. Such rarer INPs may be missed or over accounted for if only one test is conducted. The cooling rate was variable during each test, but maintained within the 1 – 10 °C min^{-1} range and the fraction frozen did not show a noticeable dependence on the cooling rate, as discussed above.

From the fraction of drops frozen and the known total volume of air per sample, we calculated the estimated INP concentration (L^{-1} of air) with the universally applied equation by Vali (1971):

$$[INP](L^{-1}) = \frac{\ln(1-f)}{V_{drop}} \times \frac{V_{suspension}}{V_{air}}$$

where f is the proportion of droplets frozen, V_{drop} is the volume of each drop, $V_{suspension}$ is the volume of the suspension (i.e., 2.5 mL for the sample tests), and V_{air} is the volume of air per sample.

2.3.2 Raman microscopy for deposition mode ice nucleation

Depositional ice nucleation was measured using a Nicolet Almega XR Dispersive Raman Spectrometer outfitted with a Linkham THMS600 environmental cell and a Buck Research CR-1A chilled-mirror hygrometer. The Raman spectrometer was coupled with an Olympus BX51 research-grade optical microscope with 10x, 20x, and 50x magnification abilities. The environmental cell and CR-1A hygrometer allow for temperature control and dew/frost point measurements to back calculate saturation ice ratios, S_{ice}. The environmental cell was connected to two UHP grade N_2 tanks, one is humidified and the other is a "dry" tank that is not humidified. These two were then mixed, fed through the environmental cell, and lastly the CR-1A measures the dew/frost point. In these experiments, the water vapour was kept constant while the temperature was decreased, which resulted in an increase in S_{ice}. This experimental set up, calibration, and calculation is explained in more in detail in Baustian et al. (2010), Schill and Tolbert (2013), and Primm et al. (2017).

Atmos. Meas. Tech. Discuss., https://doi.org/10.5194/amt-2018-47
Manuscript under review for journal Atmos. Meas. Tech.
Discussion started: 23 February 2018

Atmospheric Measurement Techniques Discussions

An aliquot of the solutions from the previous immersion mode experiments were used for deposition mode ice nucleation experiments (i.e., untested sample solution). The solution derived from each spot on the collected filter sample was nebulized onto a fused silica disc, which was then placed into the environmental cell at ~0% RH to allow for evaporation of water from the particles. The temperature was then decreased at a rate of 0.1 K min^{-1}, while water vapour was held constant. Temperature and dew point were recorded during the entire experiment. S_{ice} was determined from the temperature and dew point where ice was first visually identified. The different S_{ice} values at different temperatures were determined by performing the same procedure, but changing the starting water vapour pressure. This difference in water vapour pressure changes the S_{ice} value at different temperatures. Temperatures which were analysed for depositional ice nucleation were chosen to cover a wide range of those previously reported and relevant for several cloud regimes (Hoose and Möhler, 2012). Nebulization onto the disc resulted in 5000 – 10000 particles, with a range of 1 µm to 50 µm in diameter, deposited on the surface depending on the spot from the filter paper. Of the particles that nucleated ice, 3 – 5 particles were analysed for composition using Raman spectrometry for each sample. Because the purpose of the analysis was to prove that particles could be analysed for depositional ice nucleation using samples collected by HOVERCAT, only the first few particles that formed ice at each temperature regime were recorded. A more statistical approach (i.e., analysing more particles) to characterize the depositional INP population during the flight is outside the scope of this manuscript.

3 Results and discussion

3.1 Operation of HOVERCAT instruments during test flight

Although the ability to hover at an exact altitude was difficult due to vertical winds—which was determined by abrupt ascent or descent and horizontal transport of HOVERCAT while tracking in real-time—the system was able to profile and sample at altitudes from the ground level up to 2543 m AMSL (approximately 1053 m AGL) for 3 hours (Figure 7). The ability to control the BBFCS to execute the step-wise flight plan was difficult given the winds and the several-second delay in time when venting or dropping ballast to decrease or increase in altitude, respectively. Minor fluctuations in BBFCS control to maintain altitude was not possible during 25 May conditions, but may be on a calmer day aloft. Because of such issues, the first two profiles during the first hour of flight (up to 2316 and 2543 m AMSL) were abrupt and parking at desired altitudes was not achieved. We were able to hover at ~1800 m AMSL during the third profile (08:00 – 09:00), with a short drop in altitude around 08:50. Starting at 09:10, we were able to hover just above the ground at ~1500 m AMSL, with a final profile up to 2098 m AMSL at 09:25. Ultimately, the balloon deflated and ended the flight at 09:36.

While controlling the exact altitude of the BBFCS was difficult, the aerosol measurements were fruitful. The OPC measured particle concentrations up to 250 cm^{-3} while at the ground, with the lowest concentrations occurring at the highest altitudes (< 1 to 2 cm^{-3}). PM concentrations followed a similar inverse relationship with altitude (Figure 7). The total flow though the

filter in TRAPS was fairly consistent throughout the flight, starting at 40 L for Sample 1 and decreasing to 32 L for Sample 6. The slight decrease possibly resulted from: 1) inconsistent power supply by the battery pack to the micropump or 2) strain on the micropump with altitude, although the latter is less likely given the variability in altitude throughout the flight.

3.2 Immersion freezing ice nucleation

From the six filter sample spots that were collected, aerosol loading was sufficient to conduct INP measurements using the DFCP system. Cumulative INP spectra show relatively low concentrations (i.e., 10^{-2} – 10^{-1} L^{-1}) of warm temperature INPs (> −10 °C, likely of biological origin (Murray et al., 2012)) for all samples, while reaching up to 10^{1} L^{-1} at temperatures below −20 °C (Figure 8). Such concentrations are within range of those previously reported in Colorado: Prenni et al. (2013) reported 1 – 10^{2} L^{-1} at −25 °C. The highest INP concentrations were observed from Sample 3, which corresponded to the time where HOVERCAT was closest to the ground, on average (Figure 9a). Sample 6 had the highest concentrations of INPs active between −8 and −12.5 °C, which also corresponds to when HOVERCAT hovered just above ground level (Figure7). It is important to note that all samples aside from Sample 4 hovered near the ground, thus altitude-dependent results could be skewed by collection nearest to the local source of aerosol. However, based on OPC number concentrations, there was not always a clear decrease of aerosol concentrations with altitude (e.g., Sample 5). Additionally, concentrations were calculated and based on total volume of air, indicating that the altitude in which the sample was collected at for the most amount of time is representative of the overall sample INP population. Combined, the immersion INP, OPC, and BBFCS results indicate that: 1) total particle number concentrations and INP concentrations were highest closest to the ground, 2) collection at higher altitudes resulted in lower particle concentrations, and 3) INPs of likely biological origin remained close to the surface, which is predominantly agricultural soils (Hill et al., 2016). The relative abundance of INPs to total particles is also consistent with previously reported values (DeMott et al., 2010): INPs represented 1 in every 10^{2} to 10^{5} number of particles detected by the OPC, although the OPC does not measure below 380 nm so the fractions might in reality be even lower (Figure 9b). However, INPs are thought to be relatively large (i.e., > 200 nm in diameter) based on previous work (Mertes et al., 2007; DeMott et al., 2010; Fridlind et al., 2012; Niedermeier et al., 2015; Kanji et al., 2017), so the OPC may be relevant for supporting INP measurements. Although these results may not be surprising (e.g., total particle, INP concentrations within range of previous work and generally highest near the ground, and biological INPs sourced from an agricultural region) and yield results consistent with previous work (DeMott et al., 2010; Murray et al., 2012; Prenni et al., 2013; Hill et al., 2016), they demonstrate the utility and reliability of the collection and analytical methods of HOVERCAT and the DFCP systems.

3.3 Deposition freezing ice nucleation

Depositional ice nucleation analysis of the six filter samples was conducted using the extra volume of resuspension left from the immersion freezing analysis (i.e., the portion of the 2 mL that was not used on the DFCP). Overall, the samples contained

deposition INPs that enabled ice formation above homogeneous freezing. Saturation ice ratios of all six samples were similar at the temperatures tested, except for Samples 3 and 4 at approximately −40 °C (Figure 10), indicating these samples contained more efficient deposition INPs at that temperature as compared to the remaining samples. These samples contained slightly more efficient INPs at −25 °C, but similar efficiencies to the remaining samples at −55 °C. Raman spectrometry demonstrates that most of the samples were compositionally disparate from each other (Figure 11). The first three samples show a very intense fluorescence signal (i.e., the curve-like characteristic of the baseline), which is consistent with either biological or organic materials (Baustian et al., 2012). Additionally, Sample 2 contained a peak for carbonate, which is indicative of a mineral dust signature (Baustian et al., 2012). The sample collection time periods for these samples occurred directly over a dense agricultural region in the Colorado plains, supporting the observation of highly fluorescent particles (Figures 2 and 7). Interestingly, Sample 3 contained efficient immersion mode INPs as well, that were likely of biological origin due to the relatively higher INP concentrations at temperatures greater than −10 °C (Figure 8). Samples 4, 5, and 6 show a C-H stretch peak, and occasionally sulphate (SO_4^{2-}) and nitrate (NO_3^-) peaks, which is consistent with the composition of typical anthropogenic aerosols in the atmosphere (Zhang et al., 2007). Sample 5 had the most intense anthropogenic peaks while yielding the least efficient immersion mode and deposition mode (i.e., at the two highest temperatures measured) INPs. It is possible any INPs present in this sample were affected by sulphate or nitrate coatings, which have been shown to inhibit the ice nucleating abilities of aerosols (e.g., Mohler et al., 2008; Cziczo et al., 2009; Sullivan et al., 2010; Reitz et al., 2011). Collection of Samples 5 and 6 coincided with when HOVERCAT flew close to the ground near I-25, where vehicular traffic and industry lining the multilane interstate likely contributed to the larger signal from anthropogenic functional groups and less efficient INPs. However, the Raman spectrum for Sample 6 also has a weak fluorescent signature, indicating a possible biological contribution. HOVERCAT flew from over I-25 to the west over more agricultural lands. Sample 6 also contained high concentrations of INPs at – 10 °C, indicating the sample also contained biological INPs. Combined, these results from Sample 6 suggest a mixture of biological and anthropogenic sources.

3.4 Future directions for HOVERCAT

As indicated earlier, Phase I of HOVERCAT exists in its current prototype state. Plans for a Phase II to develop a more operational measurement platform are underway to: 1) improve operation at higher altitudes, 2) operate successfully on a routine basis, 3) function suitably in more extreme environments, such as in-cloud and the Arctic, 4) improve the aerosol module's versatility to adapt to other platforms such as tethered balloon systems or unmanned aerial systems (UASs), and 5) transmit data to a ground station in real-time. To improve operation for higher altitudes, modifications will be made to the micropump. The main issue is that to fly at free will (i.e., under FAA regulations), payload weight must be maintained under 2.7 kg for the aerosol module. However, more efficient yet lightweight micropumps can be used and tested in a pressurized chamber prior to deployment to improve operation at lower pressures and thus higher altitudes. Routine operations require more frequent flights and practice controlling the BBFCS to maintain a desired altitude, even in conditions with influential

vertical winds. Additionally, the aerosol module could be deployed on a launched balloon with a slow rise rate and less helium, or a reverse parachute (i.e., less buoyancy and more drag) to afford a steady vertical profile, although this eliminates the hovering capability of the system unless the free lift is adjusted such that the system may hover near inversions (i.e., < 0.5 m s^{-1}). To function in harsher environments, testing the modules in a humidified and temperature-controlled chamber is planned at temperatures down to −40 °C. Operational testing of the aerosol module in-cloud (i.e., under supersaturated and likely riming conditions) will occur at the high alpine research station in Jungfraujoch, Switzerland during spring 2018. The aerosol module may easily adapt to other platforms through modification of the foam enclosure for tethered balloons or adding a smaller, protective case to fit on small UASs. Transmitting data during flight will require an on-board computer and communications between the modules and a ground station, as is done with launched balloons. In general, several modifications are planned to improve performance, utility, and versatility of HOVERCAT for future deployments.

4 Conclusions

Here, we present a novel airborne platform called HOVERCAT that measures time- and altitude-resolved particle number and INP concentrations. The platform has the capability to hover at desired altitudes, making it an ideal system to collect sufficient aerosol loadings at a range of altitudes up to 2.6 km AMSL. Unlike similar platforms, HOVERCAT can vertically resolve particle number concentrations in addition to both immersion and deposition mode INPs. To our knowledge, this is the first platform to perform such measurements in tandem. Phase I of HOVERCAT has been successfully deployed, while ongoing efforts for improvement and modification are underway for Phase II to enable HOVERCAT to fly higher and in more inclement conditions.

The ability to evaluate vertical distributions of INP concentrations and glaciation temperatures is of crucial importance in order to inform and constrain process level models to improve understanding of aerosol-cloud interactions. Additionally, more routine measurements of INP properties are needed to understand the evolving nature of aerosol-cloud interactions under a wide range of cloud regimes, locations, and time of year.

Acknowledgements

We would like to acknowledge the Cooperative Institute for Research in Environmental Sciences at the University of Colorado, Boulder, USA for funding this work.

References

Avramov, A., Ackerman, A. S., Fridlind, A. M., van Diedenhoven, B., Botta, G., Aydin, K., Verlinde, J., Korolev, A. V., Strapp, J. W., McFarquhar, G. M., Jackson, R., Brooks, S. D., Glen, A., and Wolde, M.: Toward ice formation closure in Arctic mixed-phase boundary layer clouds during ISDAC, J Geophys Res-Atmos, 116, 2011.

Baustian, K. J., Wise, M. E., and Tolbert, M. A.: Depositional ice nucleation on solid ammonium sulfate and glutaric acid particles, Atmos. Chem. Phys., 10, 2307-2317, 2010.

Baustian, K. J., Cziczo, D. J., Wise, M. E., Pratt, K. A., Kulkarni, G., Hallar, A. G., and Tolbert, M. A.: Importance of aerosol composition, mixing state, and morphology for heterogeneous ice nucleation: A combined field and laboratory approach, J Geophys Res-Atmos, 117, 2012.

Bigg, E. K.: The Supercooling of Water, P Phys Soc Lond B, 66, 688-694, 1953.

Bigg, E. K.: Ice forming nuclei in the high Arctic, Tellus B, 48, 2011.

Boucher, O., Randall, D., Artaxo, P., Bretherton, C., Feingold, G., Forster, P., Kerminen, V.-M., Kondo, Y., Liao, H., Lohmann, U., Rasch, P., Satheesh, S. K., Sherwood, S., Stevens, B., and Zhang, X. Y.: Clouds and Aerosols, in: Climate Change 2013: The Physical Science Basis. Contribution of Working Group I to the Fifth Assessment Report of the Intergovernmental Panel on Climate Change, edited by: Stocker, T. F., Qin, D., Plattner, G.-K., Tignor, M., Allen, S. K., Boschung, J., Nauels, A., Xia, Y., Bex, V., and Midgley, P. M., Cambridge University Press, Cambridge, United Kingdom and New York, NY, USA, 571–658, 2013.

Bowers, R. M., Lauber, C. L., Wiedinmyer, C., Hamady, M., Hallar, A. G., Fall, R., Knight, R., and Fierer, N.: Characterization of Airborne Microbial Communities at a High-Elevation Site and Their Potential To Act as Atmospheric Ice Nuclei, Appl Environ Microb, 75, 5121-5130, 2009.

Chou, C., Stetzer, O., Weingartner, E., Juranyi, Z., Kanji, Z. A., and Lohmann, U.: Ice nuclei properties within a Saharan dust event at the Jungfraujoch in the Swiss Alps, Atmos Chem Phys, 11, 4725-4738, 2011.

Coluzza, I., Creamean, J., Rossi, M., Wex, H., Alpert, P., Bianco, V., Boose, Y., Dellago, C., Felgitsch, L., Fröhlich-Nowoisky, J., Herrmann, H., Jungblut, S., Kanji, Z., Menzl, G., Moffett, B., Moritz, C., Mutzel, A., Pöschl, U., Schauperl, M., Scheel, J., Stopelli, E., Stratmann, F., Grothe, H., and Schmale, D.: Perspectives on the Future of Ice Nucleation Research: Research Needs and Unanswered Questions Identified from Two International Workshops, Atmosphere-Basel, 8, 138, 2017.

Conen, F., Morris, C. E., Leifeld, J., Yakutin, M. V., and Alewell, C.: Biological residues define the ice nucleation properties of soil dust, Atmos. Chem. Phys., 11, 9643-9648, 2011.

Conen, F., Rodriguez, S., Huglin, C., Henne, S., Herrmann, E., Bukowiecki, N., and Alewell, C.: Atmospheric ice nuclei at the high-altitude observatory Jungfraujoch, Switzerland, Tellus Series B-Chemical and Physical Meteorology, 67, 2015.

Conen, F., Stopelli, E., and Zimmermann, L.: Clues that decaying leaves enrich Arctic air with ice nucleating particles, Atmospheric Environment, 129, 91-94, 2016.

Creamean, J. M., Suski, K. J., Rosenfeld, D., Cazorla, A., DeMott, P. J., Sullivan, R. C., White, A. B., Ralph, F. M., Minnis, P., Comstock, J. M., Tomlinson, J. M., and Prather, K. A.: Dust and Biological Aerosols from the Sahara and Asia Influence Precipitation in the Western U.S., Science, 339, 1572-1578, 2013.

Creamean, J. M., Lee, C., Hill, T. C., Ault, A. P., DeMott, P. J., White, A. B., Ralph, F. M., and Prather, K. A.: Chemical properties of insoluble precipitation residue particles, Journal of Aerosol Science, 76, 13-27, 2014.

Curry, J. A., Hobbs, P. V., King, M. D., Randall, D. A., and Minnis, P.: FIRE arctic clouds experiment, B Am Meteorol Soc, 81, 5-29, 2000.

Cziczo, D. J., DeMott, P. J., Brooks, S. D., Prenni, A. J., Thomson, D. S., Baumgardner, D., Wilson, J. C., Kreidenweis, S. M., and Murphy, D. M.: Observations of organic species and atmospheric ice formation, Geophys Res Lett, 31, 2004.

Cziczo, D. J., Froyd, K. D., Gallavardin, S. J., Moehler, O., Benz, S., Saathoff, H., and Murphy, D. M.: Deactivation of ice nuclei due to atmospherically relevant surface coatings, Environ Res Lett, 4, 2009.

Cziczo, D. J., Ladino, L., Boose, Y., Kanji, Z. A., Kupiszewski, P., Lance, S., Mertes, S., and Wex, H.: Measurements of Ice Nucleating Particles and Ice Residuals, Meteorological Monographs, 58, 8.1-8.13, 2017.

de Boer, G., Ivey, M., Schmid, B., Lawrence, D., Dexheimer, D., Mei, F., Hubbe, J., Bendure, A., Hardesty, J., Shupe, M. J., McComiskey, A., Telg, H., Schmitt, C., Matrosov, S., Brooks, I., Creamean, J. M., Solomon, A., Turner, D. D., Williams, C., Maahn, M., Argrow, B., Palo, S., Long, C. N., Gao, R.-S., and Mather, J.: A Bird's Eye View: Development of an Operational ARM Unmanned Aerial Systems Capability for Atmospheric Research in Arctic Alaska, B Am Meteorol Soc, under review, 2018.

DeMott, P. J., Chen, Y., Kreidenweis, S. M., Rogers, D. C., and Sherman, D. E.: Ice formation by black carbon particles, Geophys Res Lett, 26, 2429-2432, 1999.

DeMott, P. J., Sassen, K., Poellot, M. R., Baumgardner, D., Rogers, D. C., Brooks, S. D., Prenni, A. J., and Kreidenweis, S. M.: African dust aerosols as atmospheric ice nuclei, Geophys Res Lett, 30, 2003.

DeMott, P. J., Prenni, A. J., Liu, X., Kreidenweis, S. M., Petters, M. D., Twohy, C. H., Richardson, M. S., Eidhammer, T., and Rogers, D. C.: Predicting global atmospheric ice nuclei distributions and their impacts on climate, P Natl Acad Sci USA, 107, 11217-11222, 2010.

DeMott, P. J., Hill, T. C. J., McCluskey, C. S., Prather, K. A., Collins, D. B., Sullivan, R. C., Ruppel, M. J., Mason, R. H., Irish, V. E., Lee, T., Hwang, C. Y., Rhee, T. S., Snider, J. R., McMeeking, G. R., Dhaniyala, S., Lewis, E. R., Wentzell, J. J. B., Abbatt, J., Lee, C., Sultana, C. M., Ault, A. P., Axson, J. L., Martinez, M. D., Venero, I., Santos-Figueroa, G., Stokes, M. D., Deane, G. B.,

Mayol-Bracero, O. L., Grassian, V. H., Bertram, T. H., Bertram, A. K., Moffett, B. F., and Franc, G. D.: Sea spray aerosol as a unique source of ice nucleating particles, P Natl Acad Sci USA, 113, 5797-5803, 2016.

Despres, V. R., Huffman, J. A., Burrows, S. M., Hoose, C., Safatov, A. S., Buryak, G., Frohlich-Nowoisky, J., Elbert, W., Andreae, M. O., Poschl, U., and Jaenicke, R.: Primary biological aerosol particles in the atmosphere: a review, Tellus Series B-Chemical and Physical Meteorology, 64, 2012.

Durant, A. J., Shaw, R. A., Rose, W. I., Mi, Y., and Ernst, G. G. J.: Ice nucleation and overseeding of ice in volcanic clouds, Journal of Geophysical Research: Atmospheres, 113, n/a-n/a, 2008.

Fridlind, A. M., Diedenhoven, B. v., Ackerman, A. S., Avramov, A., Mrowiec, A., Morrison, H., Zuidema, P., and Shupe, M. D.: A FIRE-ACE/SHEBA Case Study of Mixed-Phase Arctic Boundary Layer Clouds: Entrainment Rate Limitations on Rapid Primary Ice Nucleation Processes, J Atmos Sci, 69, 365-389, 2012.

Garcia, E., Hill, T. C. J., Prenni, A. J., DeMott, P. J., Franc, G. D., and Kreidenweis, S. M.: Biogenic ice nuclei in boundary layer air over two U.S. High Plains agricultural regions, J Geophys Res-Atmos, 117, 2012.

Greenberg, J. R., Guenther, A. B., and Turnipseed, A.: Tethered balloon-based soundings of ozone, aerosols, and solar radiation near Mexico City during MIRAGE-MEX, Atmospheric Environment, 43, 2672-2677, 2009.

Hader, J. D., Wright, T. P., and Petters, M. D.: Contribution of pollen to atmospheric ice nuclei concentrations, Atmos Chem Phys, 14, 5433-5449, 2014.

Hanlon, R., Powers, C., Failor, K., Monteil, C. L., Vinatzer, B. A., and Schmale, D. G.: Microbial ice nucleators scavenged from the atmosphere during simulated rain events, Atmospheric Environment, 163, 182-189, 2017.

Hara, K., Osada, K., Nishita-Hara, C., and Yamanouchi, T.: Seasonal variations and vertical features of aerosol particles in the Antarctic troposphere, Atmos Chem Phys, 11, 5471-5484, 2011.

Hill, T. C. J., DeMott, P. J., Tobo, Y., Fröhlich-Nowoisky, J., Moffett, B. F., Franc, G. D., and Kreidenweis, S. M.: Sources of organic ice nucleating particles in soils, Atmos. Chem. Phys., 16, 7195-7211, 2016.

Hofmann, D. J., Rosen, J. M., Harder, J. W., and Hereford, J. V.: Balloon-borne measurements of aerosol, condensation nuclei, and cloud particles in the stratosphere at McMurdo Station, Antarctica, during the spring of 1987, Journal of Geophysical Research: Atmospheres, 94, 11253-11269, 1989.

Hofmann, D. J.: Twenty years of balloon-borne tropospheric aerosol measurements at Laramie, Wyoming, Journal of Geophysical Research: Atmospheres, 98, 12753-12766, 1993.

Hoose, C., and Möhler, O.: Heterogeneous ice nucleation on atmospheric aerosols: a review of results from laboratory experiments, Atmos. Chem. Phys., 12, 9817-9854, 2012.

Huffman, J. A., Prenni, A. J., DeMott, P. J., Pohlker, C., Mason, R. H., Robinson, N. H., Frohlich-Nowoisky, J., Tobo, Y., Despres, V. R., Garcia, E., Gochis, D. J., Harris, E., Mueller-Germann, I., Ruzene, C., Schmer, B., Sinha, B., Day, D. A., Andreae, M. O., Jimenez, J. L., Gallagher, M., Kreidenweis, S. M., Bertram, A. K., and Poschl, U.: High concentrations of biological aerosol particles and ice nuclei during and after rain, Atmos Chem Phys, 13, 6151-6164, 2013.

Irish, V. E., Elizondo, P., Chen, J., Chou, C., Charette, J., Lizotte, M., Ladino, L. A., Wilson, T. W., Gosselin, M., Murray, B. J., Polishchuk, E., Abbatt, J. P. D., Miller, L. A., and Bertram, A. K.: Ice-nucleating particles in Canadian Arctic sea-surface microlayer and bulk seawater, Atmos Chem Phys, 17, 10583-10595, 2017.

Iwasaka, Y., Shi, G.-Y., Shen, Z., Kim, Y. S., Trochkine, D., Matsuki, A., Zhang, D., Shibata, T., Nagatani, M., and Nakata, H.: Nature of Atmospheric Aerosols over the Desert Areas in the Asian Continent: Chemical State and Number Concentration of Particles Measured at Dunhuang, China, Water, Air and Soil Pollution: Focus, 3, 129-145, 2003.

Jayaweera, K., and Flanagan, P.: Investigations on Biogenic Ice Nuclei in the Arctic Atmosphere, Geophys Res Lett, 9, 94-97, 1982.

Joly, M., Attard, E., Sancelme, M., Deguillaume, L., Guilbaud, C., Morris, C. E., Amato, P., and Delort, A. M.: Ice nucleation activity of bacteria isolated from cloud water, Atmospheric Environment, 70, 392-400, 2013.

Joly, M., Amato, P., Deguillaume, L., Monier, M., Hoose, C., and Delort, A. M.: Quantification of ice nuclei active at near 0 degrees C temperatures in low-altitude clouds at the Puy de Dome atmospheric station, Atmos Chem Phys, 14, 8185-8195, 2014.

Kanji, Z. A., Ladino, L. A., Wex, H., Boose, Y., Burkert-Kohn, M., Cziczo, D. J., and Krämer, M.: Overview of Ice Nucleating Particles, Meteorological Monographs, 58, 1.1-1.33, 2017.

Kim, Y. S., Iwasaka, Y., Shi, G.-Y., Shen, Z., Trochkine, D., Matsuki, A., Zhang, D., Shibata, T., Nagatani, M., and Nakata, H.: Features in Number Concentration-Size Distributions of Aerosols in the Free Atmosphere over the Desert Areas in the Asian Continent: Balloon-Borne Measurements at Dunhuang, China, Water, Air and Soil Pollution: Focus, 3, 147-159, 2003.

Langham, E. J., and Mason, B. J.: The Heterogeneous and Homogeneous Nucleation of Supercooled Water, Proc R Soc Lon Ser-A, 247, 493-&, 1958.

Maletto, A., McKendry, I. G., and Strawbridge, K. B.: Profiles of particulate matter size distributions using a balloon-borne lightweight aerosol spectrometer in the planetary boundary layer, Atmospheric Environment, 37, 661-670, 2003.

Mason, R. H., Si, M., Li, J., Chou, C., Dickie, R., Toom-Sauntry, D., Pohlker, C., Yakobi-Hancock, J. D., Ladino, L. A., Jones, K., Leaitch, W. R., Schiller, C. L., Abbatt, J. P. D., Huffman, J. A., and Bertram, A. K.: Ice nucleating particles at a coastal marine boundary layer site: correlations with aerosol type and meteorological conditions, Atmos Chem Phys, 15, 12547-12566, 2015.

McCluskey, C. S., DeMott, P. J., Prenni, A. J., Levin, E. J. T., McMeeking, G. R., Sullivan, A. P., Hill, T. C. J., Nakao, S., Carrico, C. M., and Kreidenweis, S. M.: Characteristics of atmospheric ice nucleating particles associated with biomass burning in the US: Prescribed burns and wildfires, Journal of Geophysical Research: Atmospheres, 119, 10458-10470, 2014.

Mertes, S., Verheggen, B., Walter, S., Connolly, P., Ebert, M., Schneider, J., Bower, K. N., Cozic, J., Weinbruch, S., Baltensperger, U., and Weingartner, E.: Counterflow Virtual Impactor Based Collection of Small Ice Particles in Mixed-Phase Clouds for the Physico-Chemical Characterization of Tropospheric Ice Nuclei: Sampler Description and First Case Study, Aerosol Science and Technology, 41, 848-864, 2007.

Moffett, B. F.: Fresh water ice nuclei, Fund Appl Limnol, 188, 19-23, 2016.

Mohler, O., Benz, S., Saathoff, H., Schnaiter, M., Wagner, R., Schneider, J., Walter, S., Ebert, V., and Wagner, S.: The effect of organic coating on the heterogeneous ice nucleation efficiency of mineral dust aerosols, Environ Res Lett, 3, 2008.

Morrison, H., Shupe, M. D., Pinto, J. O., and Curry, J. A.: Possible roles of ice nucleation mode and ice nuclei depletion in the extended lifetime of Arctic mixed-phase clouds, Geophys Res Lett, 32, 2005.

Mossop, S. C.: Atmospheric Ice Nuclei, Z Angew Math Phys, 14, 456-+, 1963.

Mossop, S. C., and Thorndike, N. S. C.: The Use of Membrane Filters in Measurements of Ice Nucleus Concentration. I. Effect of Sampled Air Volume, Journal of Applied Meteorology, 5, 474-480, 1966.

Murray, B. J., O'Sullivan, D., Atkinson, J. D., and Webb, M. E.: Ice nucleation by particles immersed in supercooled cloud droplets, Chem Soc Rev, 41, 6519-6554, 2012.

Niedermeier, D., Augustin-Bauditz, S., Hartmann, S., Wex, H., Ignatius, K., and Stratmann, F.: Can we define an asymptotic value for the ice active surface site density for heterogeneous ice nucleation?, Journal of Geophysical Research: Atmospheres, 120, 5036-5046, 2015.

O'Sullivan, D., Murray, B. J., Malkin, T. L., Whale, T. F., Umo, N. S., Atkinson, J. D., Price, H. C., Baustian, K. J., Browse, J., and Webb, M. E.: Ice nucleation by fertile soil dusts: relative importance of mineral and biogenic components, Atmos Chem Phys, 14, 1853-1867, 2014.

Ogren, J. A., Wendell, J., Andrews, E., and Sheridan, P. J.: Continuous light absorption photometer for long-term studies, Atmos Meas Tech, 10, 4805-4818, 2017.

Petters, M. D., Parsons, M. T., Prenni, A. J., DeMott, P. J., Kreidenweis, S. M., Carrico, C. M., Sullivan, A. P., McMeeking, G. R., Levin, E., Wold, C. E., Collett, J. L., and Moosmüller, H.: Ice nuclei emissions from biomass burning, Journal of Geophysical Research: Atmospheres, 114, n/a-n/a, 2009.

Petters, M. D., and Wright, T. P.: Revisiting ice nucleation from precipitation samples, Geophys Res Lett, 42, 8758-8766, 2015.

Pietsch, R. B., Vinatzer, B. A., and Schmale, D. G.: Diversity and Abundance of Ice Nucleating Strains of Pseudomonas syringae in a Freshwater Lake in Virginia, USA, Front Microbiol, 8, 2017.

Polen, M., Lawlis, E., and Sullivan, R. C.: The unstable ice nucleation properties of Snomax® bacterial particles, Journal of Geophysical Research: Atmospheres, 121, 11,666-611,678, 2016.

Pouzet, G., Peghaire, E., Agues, M., Baray, J. L., Conen, F., and Amato, P.: Atmospheric Processing and Variability of Biological Ice Nucleating Particles in Precipitation at Opme, France, Atmosphere-Basel, 8, 2017.

Pratt, K. A., DeMott, P. J., French, J. R., Wang, Z., Westphal, D. L., Heymsfield, A. J., Twohy, C. H., Prenni, A. J., and Prather, K. A.: In situ detection of biological particles in cloud ice-crystals, Nat Geosci, 2, 397-400, 2009.

Prenni, A. J., Demott, P. J., Rogers, D. C., Kreidenweis, S. M., Mcfarquhar, G. M., Zhang, G., and Poellot, M. R.: Ice nuclei characteristics from M-PACE and their relation to ice formation in clouds, Tellus Series B-Chemical and Physical Meteorology, 61, 436-448, 2009a.

Prenni, A. J., Petters, M. D., Kreidenweis, S. M., Heald, C. L., Martin, S. T., Artaxo, P., Garland, R. M., Wollny, A. G., and Poschl, U.: Relative roles of biogenic emissions and Saharan dust as ice nuclei in the Amazon basin, Nat Geosci, 2, 401-404, 2009b.

Prenni, A. J., Tobo, Y., Garcia, E., DeMott, P. J., Huffman, J. A., McCluskey, C. S., Kreidenweis, S. M., Prenni, J. E., Pohlker, C., and Poschl, U.: The impact of rain on ice nuclei populations at a forested site in Colorado, Geophys Res Lett, 40, 227-231, 2013.

Primm, K. M., Schill, G. P., Veghte, D. P., Freedman, M. A., and Tolbert, M. A.: Depositional ice nucleation on NX illite and mixtures of NX illite with organic acids, J Atmos Chem, 74, 55-69, 2017.

Pruppacher, H. R., and Klett, J. D.: Microphysics of Clouds and Precipitation, Atmospheric and Oceanographic Sciences Library, Kluwer Academic Publishers, Dordrecht, The Netherlands, 1997.

Rankin, A. M., and Wolff, E. W.: Aerosol profiling using a tethered balloon in coastal Antarctica, J Atmos Ocean Tech, 19, 1978-1985, 2002.

Reitz, P., Spindler, C., Mentel, T. F., Poulain, L., Wex, H., Mildenberger, K., Niedermeier, D., Hartmann, S., Clauss, T., Stratmann, F., Sullivan, R. C., DeMott, P. J., Petters, M. D., Sierau, B., and Schneider, J.: Surface modification of mineral dust particles by sulphuric acid processing: implications for ice nucleation abilities, Atmos. Chem. Phys., 11, 7839-7858, 2011.

Renard, J. B., Dulac, F., Berthet, G., Lurton, T., Vignelles, D., Jegou, F., Tonnelier, T., Jeannot, M., Coute, B., Akiki, R., Verdier, N., Mallet, M., Gensdarmes, F., Charpentier, P., Mesmin, S., Duverger, V., Dupont, J. C., Elias, T., Crenn, V., Sciare, J., Zieger, P., Salter, M., Roberts, T., Giacomoni, J., Gobbi, M., Hamonou, E., Olafsson, H., Dagsson-Waldhauserova, P., Camy-Peyret, C.,

Mazel, C., Decamps, T., Piringer, M., Surcin, J., and Daugeron, D.: LOAC: a small aerosol optical counter/sizer for ground-based and balloon measurements of the size distribution and nature of atmospheric particles - Part 2: First results from balloon and unmanned aerial vehicle flights, Atmos Meas Tech, 9, 3673-3686, 2016.

Richardson, M. S., DeMott, P. J., Kreidenweis, S. M., Cziczo, D. J., Dunlea, E. J., Jimenez, J. L., Thomson, D. S., Ashbaugh, L. L., Borys, R. D., Westphal, D. L., Casuccio, G. S., and Lersch, T. L.: Measurements of heterogeneous ice nuclei in the western United States in springtime and their relation to aerosol characteristics, J Geophys Res-Atmos, 112, 2007.

Rogers, D. C., DeMott, P. J., Kreidenweis, S. M., and Chen, Y. L.: Measurements of ice nucleating aerosols during SUCCESS, Geophys Res Lett, 25, 1383-1386, 1998.

Rogers, D. C., DeMott, P. J., and Kreidenweis, S. M.: Airborne measurements of tropospheric ice-nucleating aerosol particles in the Arctic spring, J Geophys Res-Atmos, 106, 15053-15063, 2001.

Schill, G. P., and Tolbert, M. A.: Heterogeneous ice nucleation on phase-separated organic-sulfate particles: effect of liquid vs. glassy coatings, Atmos Chem Phys, 13, 4681-4695, 2013.

Schnell, R. C., and Vali, G.: Atmospheric Ice Nuclei from Decomposing Vegetation, Nature, 236, 163-+, 1972.

Schnell, R. C., and Vali, G.: World-Wide Source of Leaf Derived Freezing Nuclei, Nature, 246, 212-213, 1973.

Schnell, R. C., and Vali, G.: Freezing Nuclei in Marine Waters, Tellus, 27, 321-323, 1975.

Schnell, R. C., and Vali, G.: Biogenic Ice Nuclei .1. Terrestrial and Marine Sources, J Atmos Sci, 33, 1554-1564, 1976.

Schnell, R. C.: Ice Nuclei in Seawater, Fog Water and Marine Air Off Coast of Nova-Scotia - Summer 1975, J Atmos Sci, 34, 1299-1305, 1977.

Schnell, R. C.: Airborne Ice Nucleus Measurements around the Hawaiian-Islands, J Geophys Res-Oc Atm, 87, 8886-8890, 1982.

Siebert, H., Stratmann, F., and Wehner, B.: First observations of increased ultrafine particle number concentrations near the inversion of a continental planetary boundary layer and its relation to ground-based measurements, Geophys Res Lett, 31, 2004.

Stopelli, E., Conen, F., Zimmermann, L., Alewell, C., and Morris, C. E.: Freezing nucleation apparatus puts new slant on study of biological ice nucleators in precipitation, Atmos Meas Tech, 7, 129-134, 2014.

Stopelli, E., Conen, F., Morris, C. E., Herrmann, E., Bukowiecki, N., and Alewell, C.: Ice nucleation active particles are efficiently removed by precipitating clouds, Sci Rep-Uk, 5, 2015.

Stopelli, E., Conen, F., Morris, C. E., Herrmann, E., Henne, S., Steinbacher, M., and Alewell, C.: Predicting abundance and variability of ice nucleating particles in precipitation at the high-altitude observatory Jungfraujoch, Atmos Chem Phys, 16, 8341-8351, 2016.

Stopelli, E., Conen, F., Guilbaud, C., Zopfi, J., Alewell, C., and Morris, C. E.: Ice nucleators, bacterial cells and Pseudomonas syringae in precipitation at Jungfraujoch, Biogeosciences, 14, 1189-1196, 2017.

Sullivan, R. C., Petters, M. D., DeMott, P. J., Kreidenweis, S. M., Wex, H., Niedermeier, D., Hartmann, S., Clauss, T., Stratmann, F., Reitz, P., Schneider, J., and Sierau, B.: Irreversible loss of ice nucleation active sites in mineral dust particles caused by sulphuric acid condensation, Atmos. Chem. Phys., 10, 11471-11487, 2010.

Tobo, Y., Iwasaka, Y., Shi, G. Y., Kim, Y. S., Ohashi, T., Tamura, K., and Zhang, D. Z.: Balloon-borne observations of high aerosol concentrations near the summertime tropopause over the Tibetan Plateau, Atmos Res, 84, 233-241, 2007.

Tobo, Y., DeMott, P. J., Hill, T. C. J., Prenni, A. J., Swoboda-Colberg, N. G., Franc, G. D., and Kreidenweis, S. M.: Organic matter matters for ice nuclei of agricultural soil origin, Atmos Chem Phys, 14, 8521-8531, 2014.

Tobo, Y.: An improved approach for measuring immersion freezing in large droplets over a wide temperature range, Sci Rep-Uk, 6, 2016.

Vali, G., and Stansbury, E. J.: Time-Dependent Characteristics of Heterogeneous Nucleation of Ice, Can J Phys, 44, 477-+, 1966.

Vali, G.: Quantitative Evaluation of Experimental Results an the Heterogeneous Freezing Nucleation of Supercooled Liquids, J Atmos Sci, 28, 402-409, 1971.

Vali, G., and Schnell, R. C.: Biogenic Sources of Atmospheric Ice Nuclei - Review, Eos T Am Geophys Un, 56, 994-994, 1975.

Vali, G., Christensen, M., Fresh, R. W., Galyan, E. L., Maki, L. R., and Schnell, R. C.: Biogenic Ice Nuclei .2. Bacterial Sources, J Atmos Sci, 33, 1565-1570, 1976.

Wehner, B., Siebert, H., Stratmann, F., Tuch, T., Wiedensohler, A., Petaja, T., Dal Maso, M., and Kulmala, M.: Horizontal homogeneity and vertical extent of new particle formation events, Tellus Series B-Chemical and Physical Meteorology, 59, 362-371, 2007.

Wright, T. P., and Petters, M. D.: The role of time in heterogeneous freezing nucleation, J Geophys Res-Atmos, 118, 3731-3743, 2013.

Wright, T. P., Petters, M. D., Hader, J. D., Morton, T., and Holder, A. L.: Minimal cooling rate dependence of ice nuclei activity in the immersion mode, J Geophys Res-Atmos, 118, 10535-10543, 2013.

Zhang, W. H., Yeo, B. S., Schmid, T., and Zenobi, R.: Single molecule tip-enhanced Raman spectroscopy with silver tips, J Phys Chem C, 111, 1733-1738, 2007.

Atmos. Meas. Tech. Discuss., https://doi.org/10.5194/amt-2018-47
Manuscript under review for journal Atmos. Meas. Tech.
Discussion started: 23 February 2018

Atmospheric Measurement Techniques Discussions

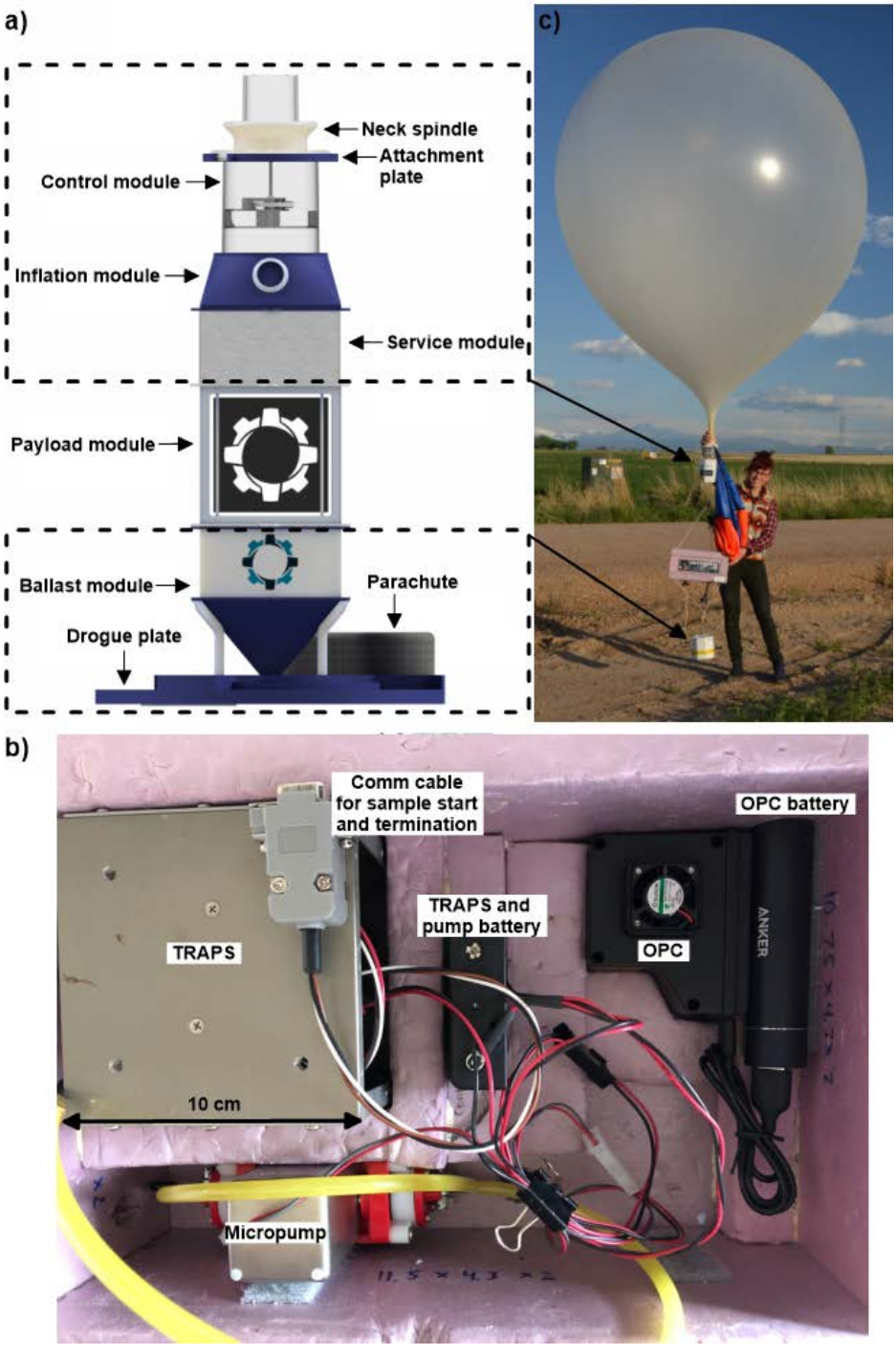

Figure 1: a) Schematic of the BBFCS. b) Picture of inside the aerosol module. c) Flight train for test flights. Note that the service module up on the BBFCS was separated approximately 1 m from the ballast module with the aerosol module (i.e., payload) in between. The ballast module was controlled by the on-board computer in the control module via an extended cable that ran down the tether string. The separated BBFCS modules were housed in foam for flights.

Atmos. Meas. Tech. Discuss., https://doi.org/10.5194/amt-2018-47
Manuscript under review for journal Atmos. Meas. Tech.
Discussion started: 23 February 2018

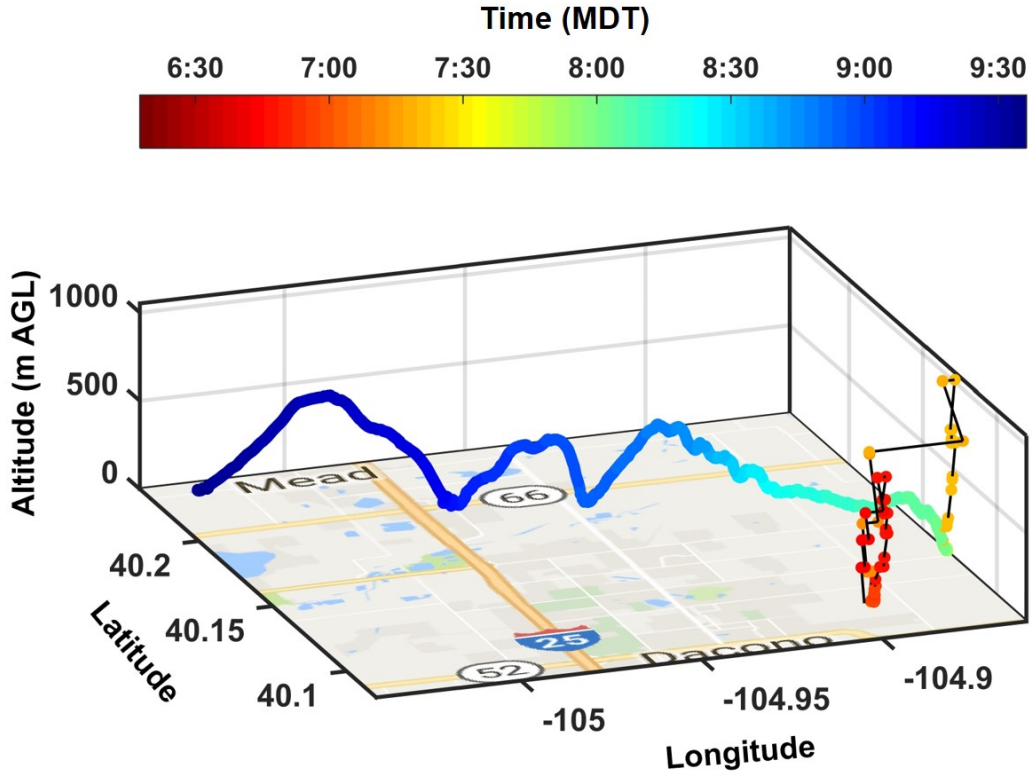

Figure 2: Four-dimensional flight path of HOVERCAT during the 25 May 2017 test flight, coloured by time in Mountain Daylight Time (MDT). Black lines between data points indicate missing GPS data, which occurred between 7:01 – 7:07 and 7:23 – 7:51. Meters AGL was calculated by subtracting 1490 from m AMSL to roughly show the altitude above ground.

Atmos. Meas. Tech. Discuss., https://doi.org/10.5194/amt-2018-47
Manuscript under review for journal Atmos. Meas. Tech.
Discussion started: 23 February 2018

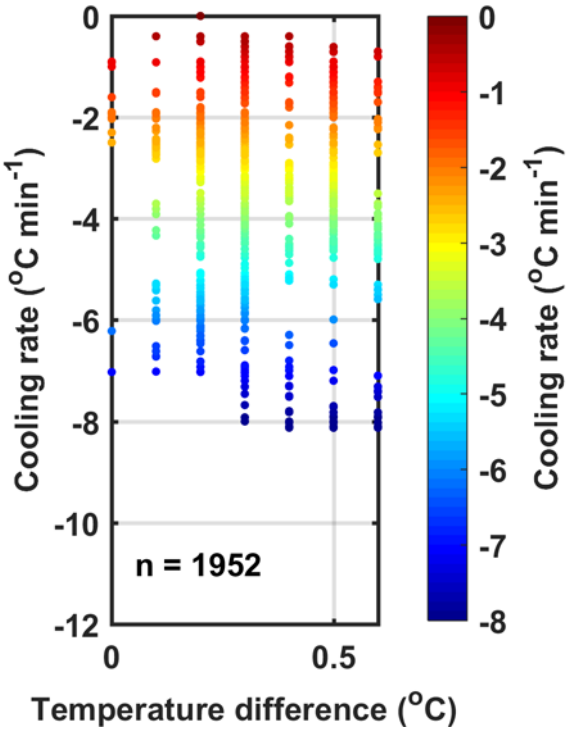

Figure 3: Temperature differences between measurements from a probe at the centre of the copper plate and drop on top of the plate coated with petrolatum. The 1-second data are from three different tests and are coloured by cooling rate. The average difference used for the temperature correction was 0.33±0.15 °C.

Atmos. Meas. Tech. Discuss., https://doi.org/10.5194/amt-2018-47
Manuscript under review for journal Atmos. Meas. Tech.
Discussion started: 23 February 2018

Atmospheric Measurement Techniques Discussions

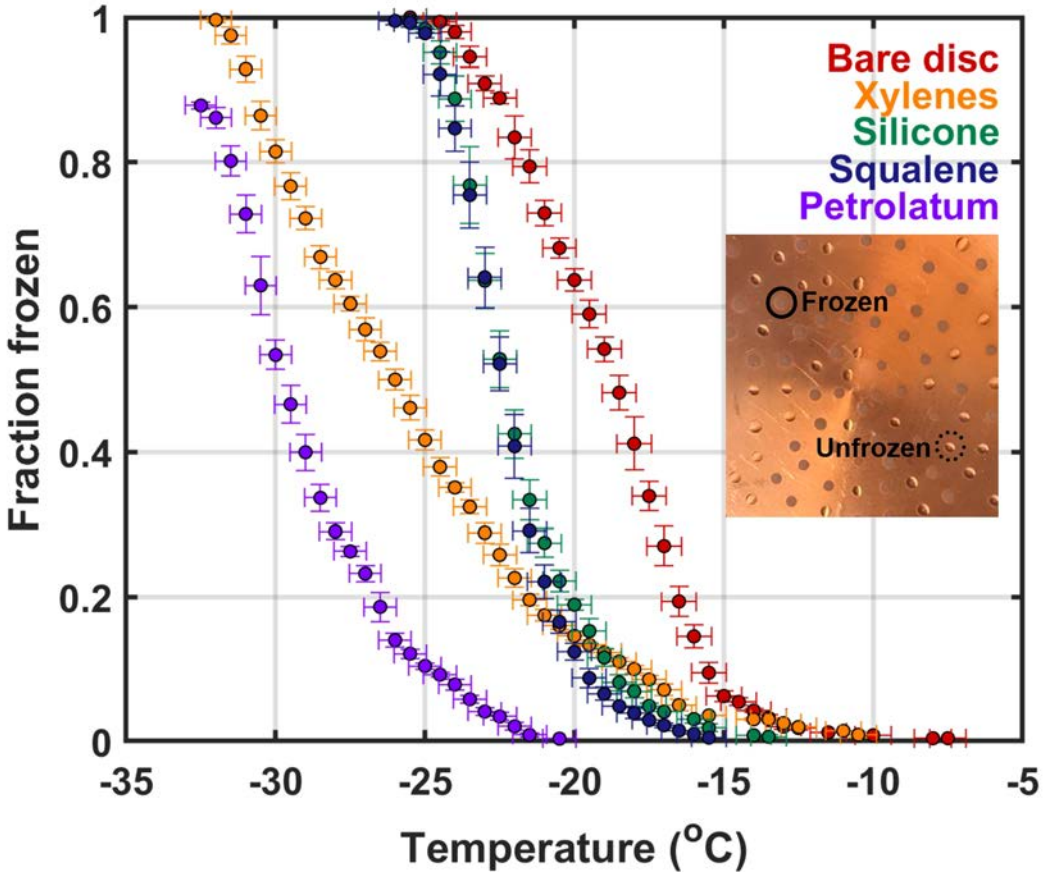

Figure 4: Freezing spectra for the control experiments conducted to characterize the DFCP system. Results included here are tests evaluating the most proficient hydrophobic coating with blank UPW drops. Error bars for the y and x axes correspond to standard deviation per 0.5 °C bin and temperature probe/plate versus drop variability standard deviation, respectively. Spectra that do not reach a frozen fraction of 1 indicates not all drops froze at the lower limit of the DFCP. The inset shows an example of the appearance of frozen versus unfrozen drops on the copper disc.

Atmos. Meas. Tech. Discuss., https://doi.org/10.5194/amt-2018-47
Manuscript under review for journal Atmos. Meas. Tech.
Discussion started: 23 February 2018

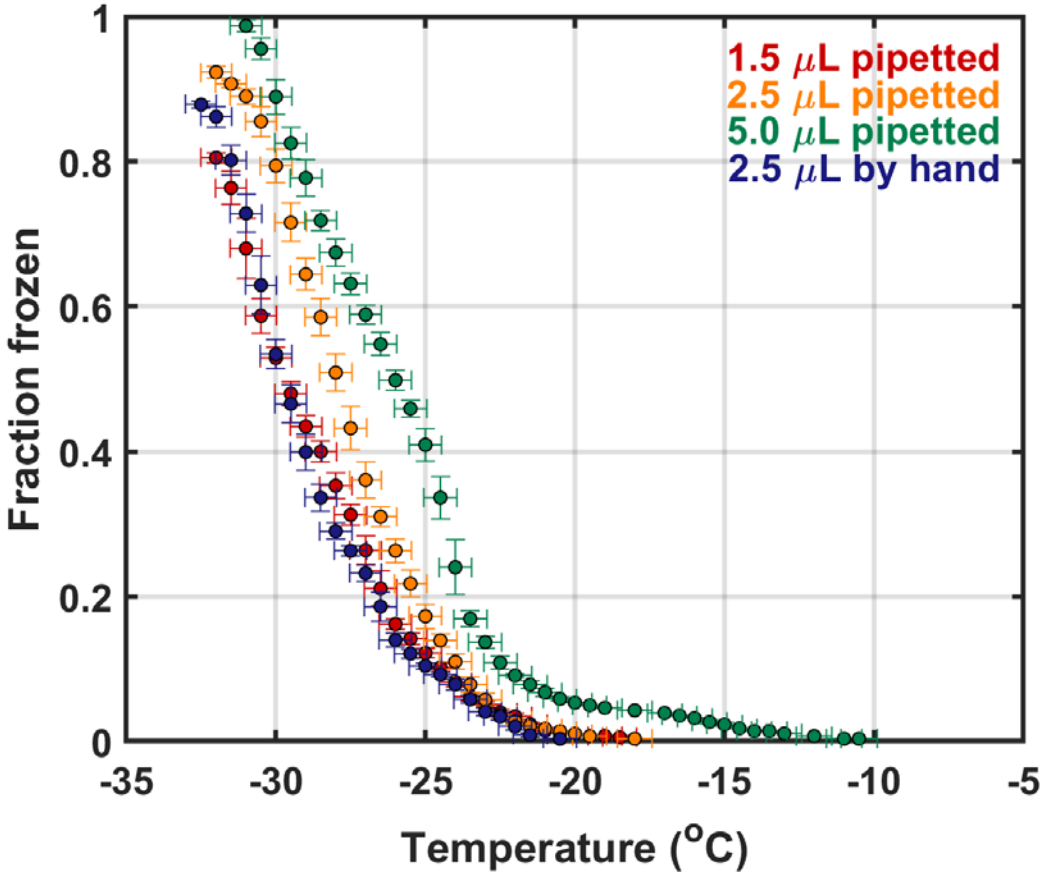

Figure 5: Freezing spectra for the control experiments conducted to characterize the drop size chosen for DFCP analysis. Results included here are tests evaluating pipetted versus hand-aliquoted drops and at different volumes. Error bars for the y and x axes correspond to standard deviation per 0.5 °C bin and temperature probe/plate versus drop variability standard deviation, respectively. Spectra that do not reach a frozen fraction of 1 indicates not all drops froze at the lower limit of the DFCP.

Atmos. Meas. Tech. Discuss., https://doi.org/10.5194/amt-2018-47
Manuscript under review for journal Atmos. Meas. Tech.
Discussion started: 23 February 2018

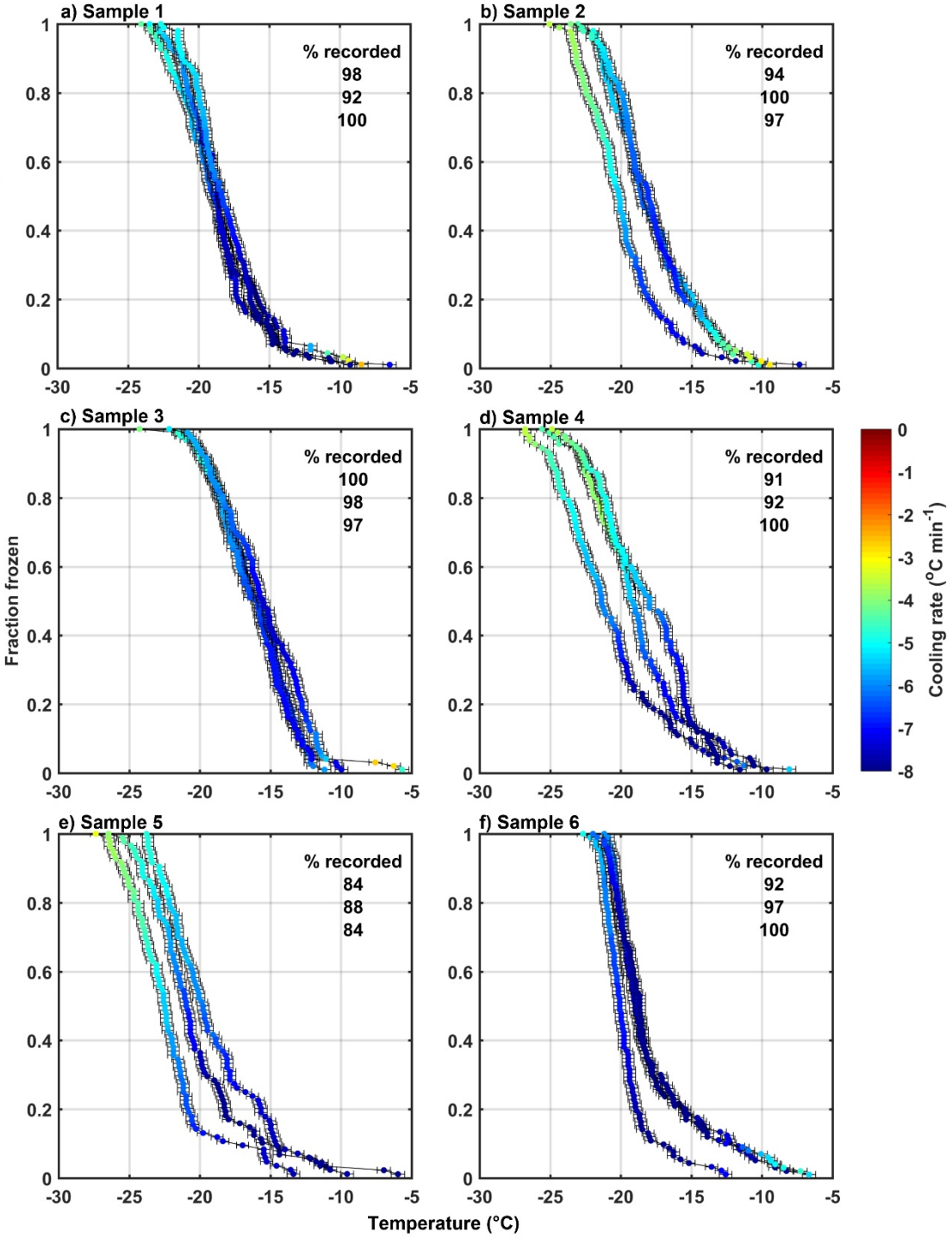

Figure 6: Freezing spectra for the three tests of each of the samples collected from HOVERCAT during the 25 May 2017 test flight. Each data point is coloured by cooling rate and has error bars associated with Omega temperature probe uncertainty. The percentage of recorded frozen drops is provided for each sample.

Atmos. Meas. Tech. Discuss., https://doi.org/10.5194/amt-2018-47
Manuscript under review for journal Atmos. Meas. Tech.
Discussion started: 23 February 2018

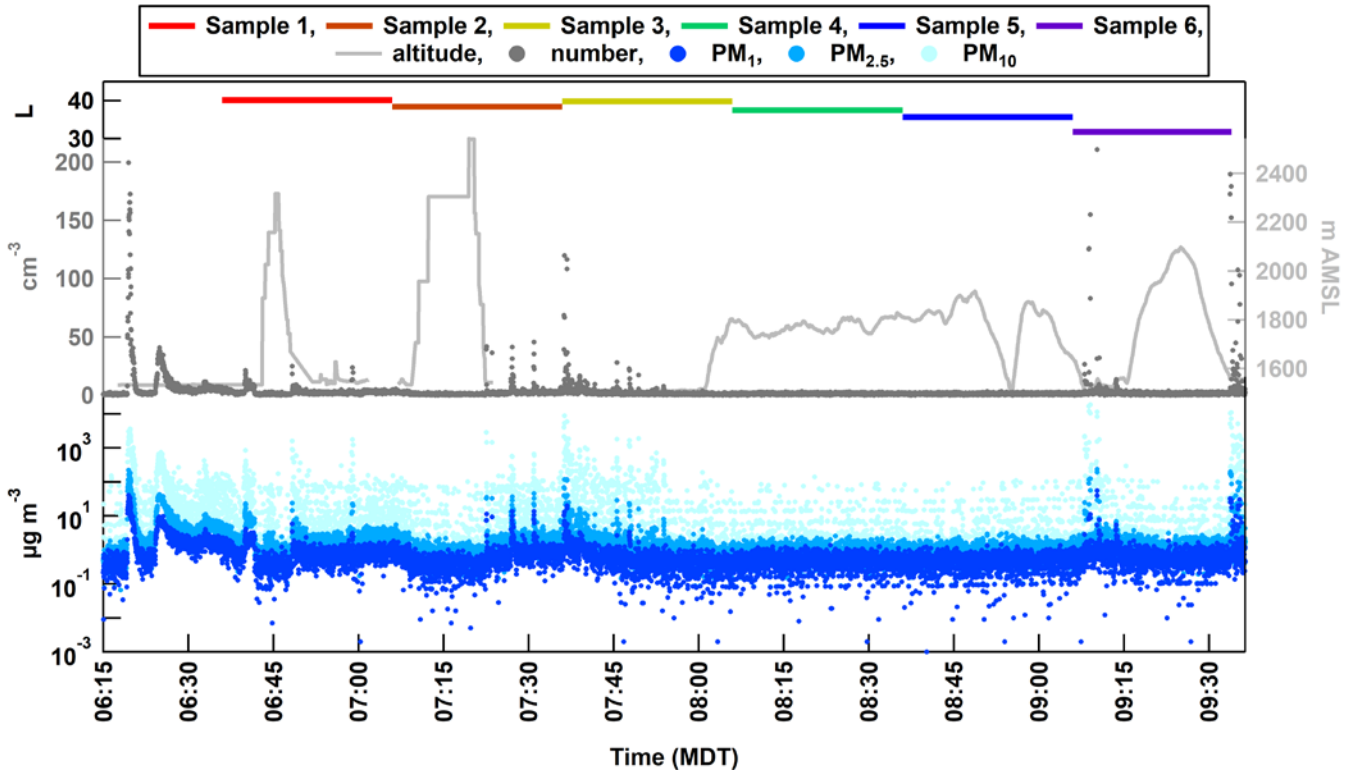

Figure 7: Time series of TRAPS total volume per sample (L; of air), OPC number concentrations (cm^{-3}), HOVERCAT altitude (m AMSL), and estimated particulate mass (PM) concentrations from the OPC (μg m^{-3}). The width of the TRAPS total volumes corresponds to the collection time per sample (i.e., 30 minutes).

Atmos. Meas. Tech. Discuss., https://doi.org/10.5194/amt-2018-47
Manuscript under review for journal Atmos. Meas. Tech.
Discussion started: 23 February 2018

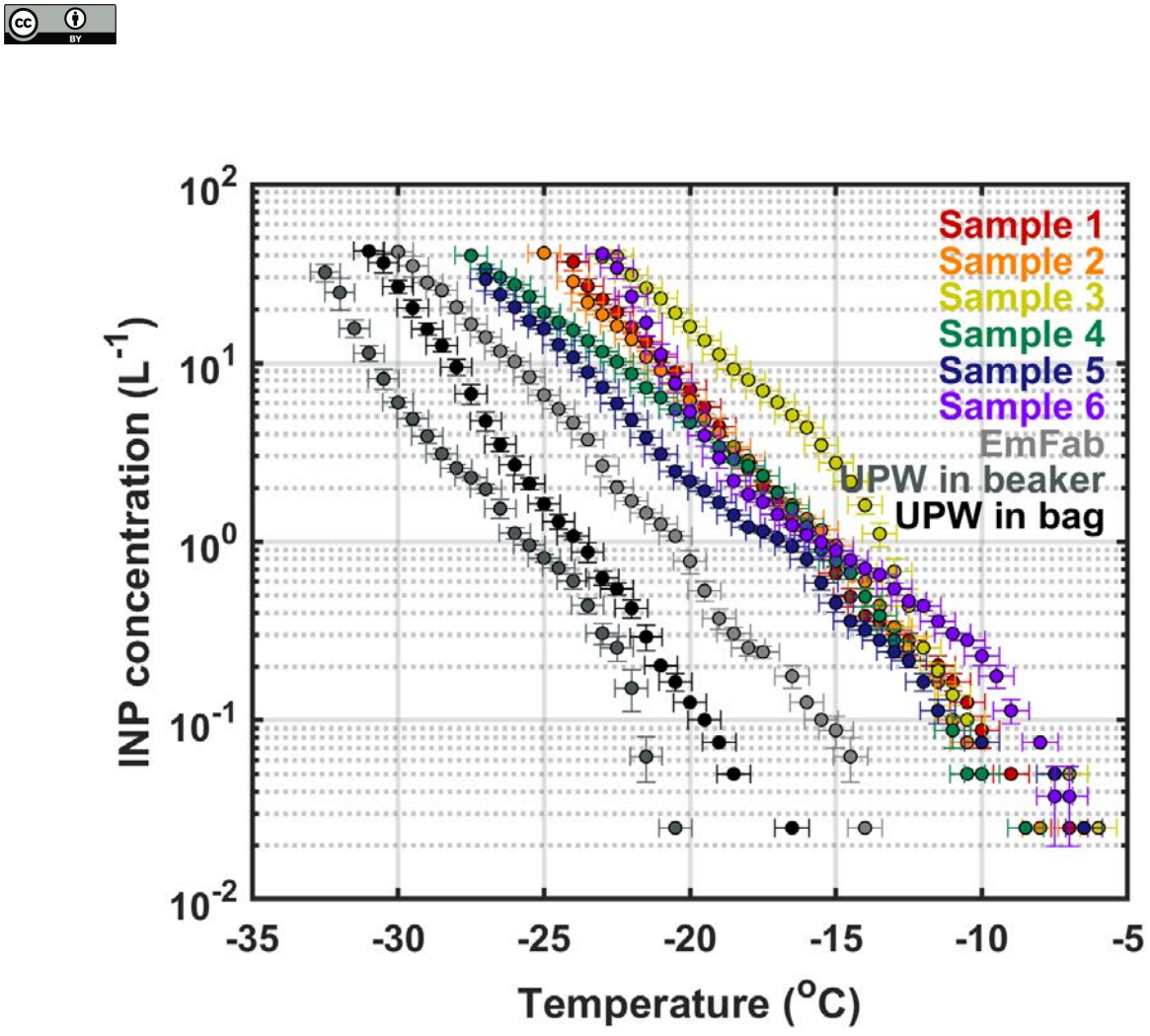

Figure 8: Cumulative INP spectra from the samples collected during the 25 May 2017 HOVERCAT test flight. Triplicate tests are binned every 0.1 °C. The blanks indicate a triplicate test from a blank UPW test and a test with EmFab™ filter prepared in UPW in the same manner as the samples. Error bars for the y and x axes correspond to standard deviation per 0.5 °C bin and temperature probe/plate versus drop variability standard deviation, respectively. Spectra that do not reach a frozen fraction of 1 indicates not all drops froze at the lower limit of the DFCP.

Atmos. Meas. Tech. Discuss., https://doi.org/10.5194/amt-2018-47
Manuscript under review for journal Atmos. Meas. Tech.
Discussion started: 23 February 2018

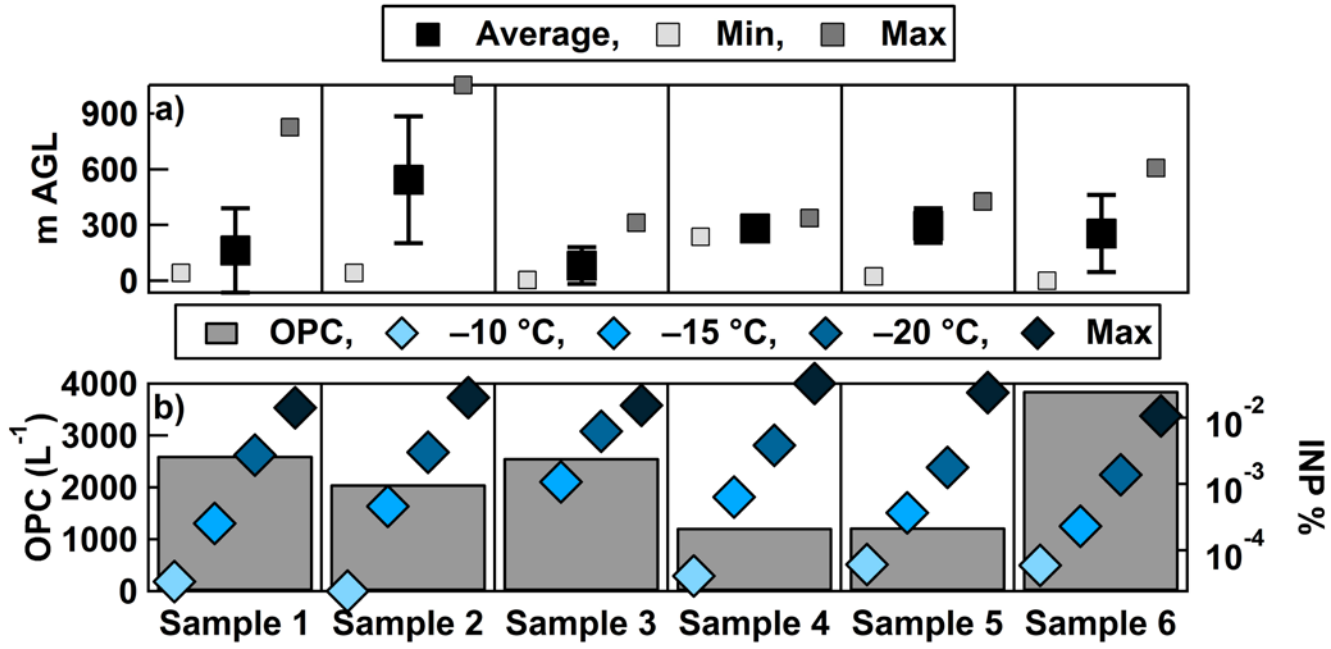

Figure 9: a) Average, minimum, and maximum altitudes HOVERCAT flew during each sample collection time period. Error bars represent one standard deviation. b) The average number concentrations of total particles from 380 nm – 17 µm in diameter measured by the OPC (left axis) and fraction of INPs out of total OPC number at −10 °C, −15 °C, −20 °C, and the maximum INP concentration measured at the temperature in which the last drop froze (right axis).

Atmos. Meas. Tech. Discuss., https://doi.org/10.5194/amt-2018-47
Manuscript under review for journal Atmos. Meas. Tech.
Discussion started: 23 February 2018

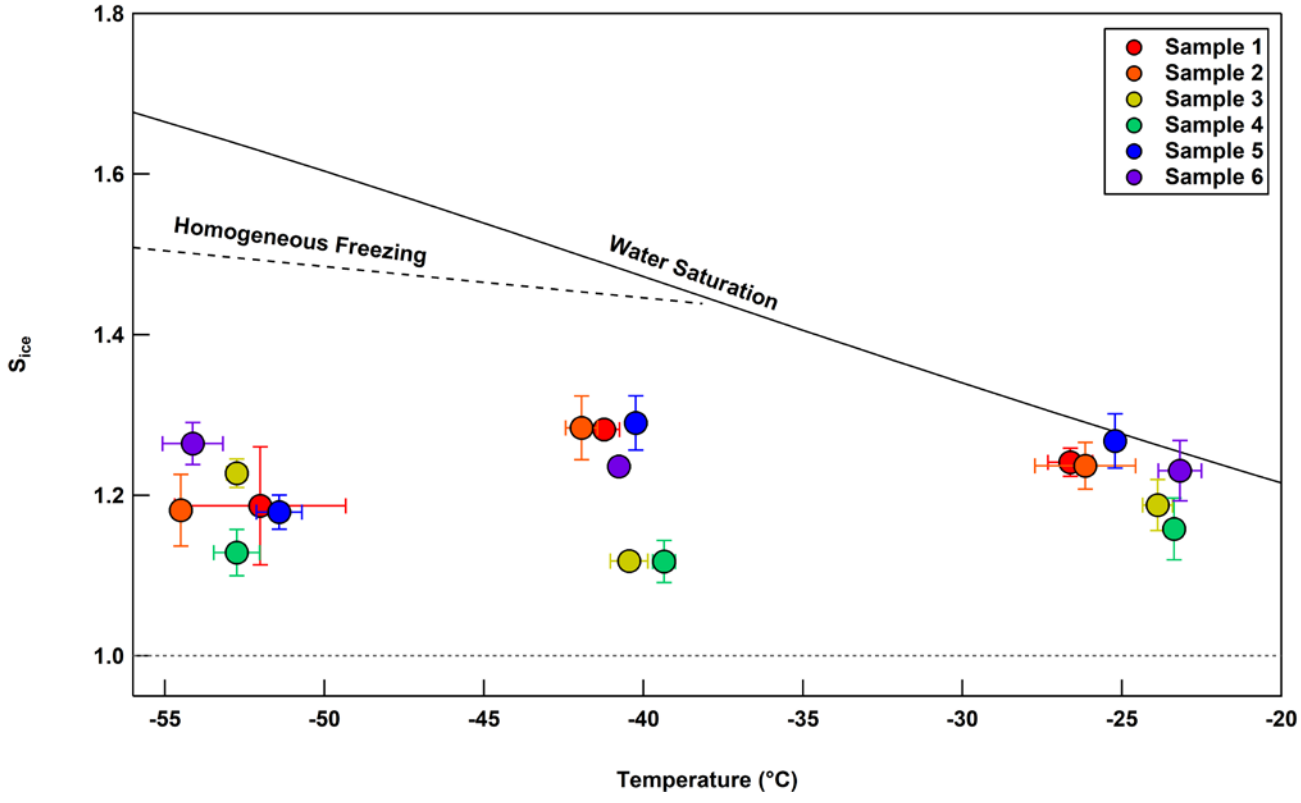

Figure 10: Depositional ice nucleation experiments on Samples 1 – 6 plotted by S_{ice} versus temperature. Although temperatures measured were not exactly −25 °C, −40 °C, and −55 °C, these values are used for brevity for all samples within each grouping shown above.

Atmos. Meas. Tech. Discuss., https://doi.org/10.5194/amt-2018-47
Manuscript under review for journal Atmos. Meas. Tech.
Discussion started: 23 February 2018

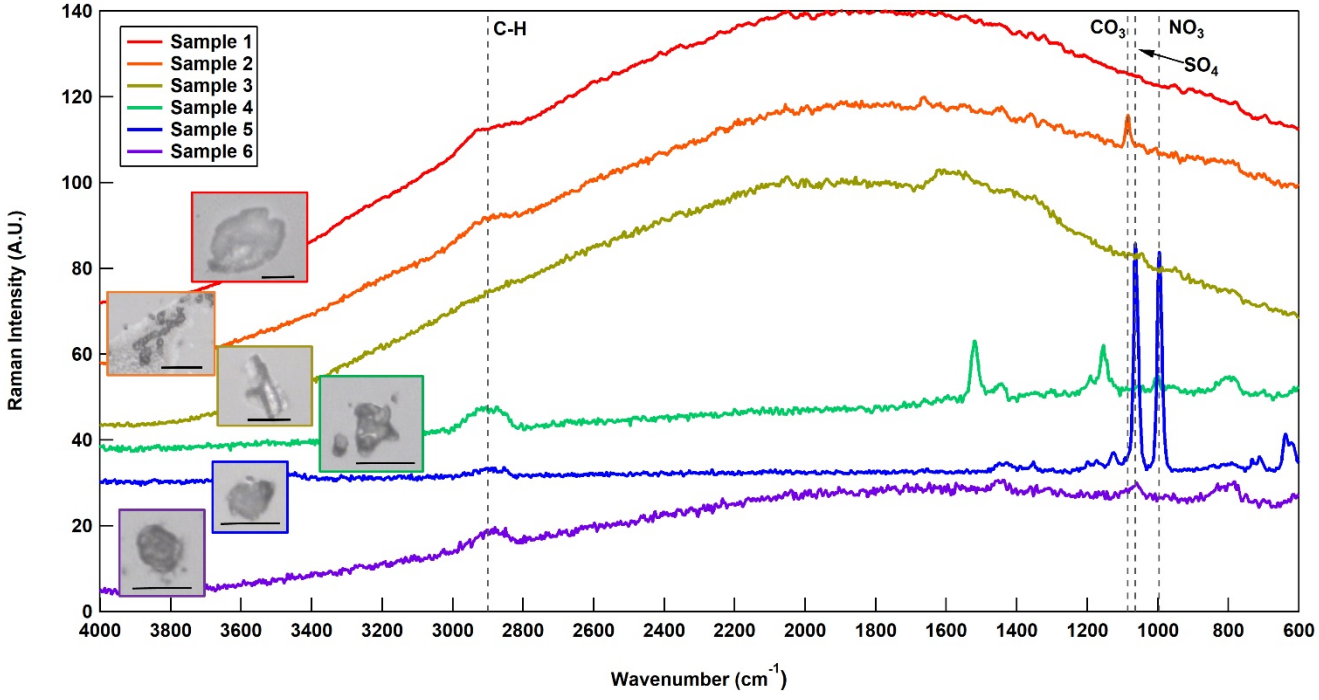

Figure 11: Raman spectra for the most representative particle type per sample. Characteristic vibrational frequencies for functional groups of organics (C-H; 2800 – 3000 cm^{-1}), carbonates (CO_3; 1070 – 1090 cm^{-1}), sulphates (SO_4; 972 – 1008 cm^{-1}), and nitrates (NO_3; 1032 – 1069 cm^{-1}) are noted for reference. Included are images of the particles that initiated depositional freezing for the Raman spectra shown. The length of the black line in each image represents a scale of 20 µm.